Measurement-induced quantum walks

A. Didi and E. Barkai

Department of Physics, Institute of Nanotechnology and Advanced Materials, Bar-Ilan University, Ramat-Gan 5290002, Israel

(Received 12 September 2021; accepted 11 April 2022; published 4 May 2022)

We investigate a tight-binding quantum walk on a graph. Repeated stroboscopic measurements of the position of the particle yield a measured "trajectory," and a combination of classical and quantum mechanical properties for the walk are observed. We explore the effects of the measurements on the spreading of the packet on a one-dimensional line, showing that except for the Zeno limit, the system converges to Gaussian statistics similarly to a classical random walk. A large deviation analysis and an Edgeworth expansion yield quantum corrections to this normal behavior. We then explore the first passage time to a target state using a generating function method, yielding properties like the quantization of the mean first return time. In particular, we study the effects of certain sampling rates that cause remarkable changes in the behavior in the system, such as divergence of the mean detection time in finite systems and decomposition of the phase space into mutually exclusive regions, an effect that mimics ergodicity breaking, whose origin here is the destructive interference in quantum mechanics. For a quantum walk on a line, we show that in our system the first detection probability decays classically like $(\text{time})^{-3/2}$. This is dramatically different compared to local measurements, which yield a decay rate of $(\text{time})^{-3}$, indicating that the exponents of the first passage time depend on the type of measurements used.

DOI: 10.1103/PhysRevE.105.054108

I. INTRODUCTION

Quantum and classical walks are by now well studied. It is well known (see details below) that a tight-binding quantum walk on a line with nearest-neighbor jumps will spread ballistically in the absence of decoherence, while the corresponding classical walk will diffuse and arrive at a Gaussian distribution. However, if we add decoherence or measurements to the quantum walk, it will converge to a classical random walk in the long time limit [1–6]. At this stage, one should ask how the convergence to the classical walk will behave. That is to say, how quickly will the system converge to the classical behavior, and more importantly, will the system truly converge to a fully classical random walk or will some traces of the original quantum behavior remain? The answer, as we demonstrate in our research, is that while the random walk will behave in a superficially classical manner, a closer examination will reveal noteworthy quantum features. These are captured with well-known tools in the statistical physics community, namely the Edgeworth expansion and large deviation theory.

In classical random walks, the spreading packet, while basic, does not yield full insight into the process. Instead, the trajectory of the random walker, and features like first passage times, occupation times, and other functionals of the path, are typically studied as they are basic in many applications [7–13]. However, when switching to the quantum world, the concept of paths is ill-defined. To better advance this issue, we study quantum walks pierced by measurements of the position operator. The results of measurements are random and yield a measured path. As an example of path properties, we consider the statistics of first hitting times. Will they resemble classical or quantum walks? We show that certain features like the mean return times for quantum walks with repeated measurements are universal, as they are quantized, independent of the structure of the graph, and, except for special measurement times, independent of the time interval between measurements. This is vastly different if compared with classical hitting times on a graph. Another noteworthy example we considered is the probability distribution of a particle on a one-dimensional lattice. Although, as expected, we found that outside the Zeno limit the measurements induce a Gaussian behavior, similar to what one would expect of a classical random walk, a closer look at the problem using large-deviation theory and an Edgeworth expansion reveals the quantum nature of the process. These results and others that we will explore in this paper demonstrate that although the process becomes a mostly classical one as a result of the repeated strong measurements, nontrivial quantum effects still arise.

To more precisely define our model, we examine a closed quantum system that is prepared in some definite initial state and evolves unitarily for a predetermined time τ, at which point we measure its position. The free evolution between measurements is given by unitary dynamics determined by the Hamiltonian of the system, typically described by the adjacency matrix of a graph. After the measurement is complete, we log the location that we found the particle in and then allow it to freely evolve for τ time once more, before repeating the process, such as in the case presented in Fig. 1. Our goals in this work are twofold: to better understand the statistical properties of such a process were it to repeat indefinitely, and to examine the first detection statistics when we are interested in the amount of time it will take for the system to reach a certain state under this measurement protocol.

The rest of the paper is organized as follows: In Secs. II and III we define our model with regard to both the

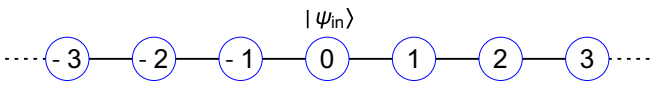

FIG. 1. A segment of the infinite line. For a particle starting at the origin, we allow it to unitarily evolve for τ time, and then we measure its position. The measurement localizes its wave function to some single site on the lattice, which we record as being the location of the particle at time τ. After this, we allow the particle to freely evolve for τ time once more before we measure its position again. By repeating this process many times, we generate a "path" that the particle took. For the lattice shown here, an example of a path would be $\{0, 2, 1, 0, -3, \dots\}$.

measurement-induced quantum random walk without termination and the first detection problem. In Sec. IV we describe the mathematical framework we will be using, and in Secs. V and VI we use it to derive several properties of this type of random walk. In Sec. VII we apply the aforementioned results and mathematical tools to study a measurement-induced quantum random walk finite graph in detail, and in Sec. VIII we do the same for an infinite one-dimensional (1D) lattice. We follow this up in Sec. IX with a comparison of our measurement scheme to a local measurement model such as the one considered in [14], as these models have seen extensive research in papers by Dhar *et al.* [15,16], Krovi and Brun [17,18], and others. In particular, we will focus on directly comparing our results to those found for the scheme considered in [19–21]. We close the paper with discussions and a summary in Sec. X. Detailed calculations and an additional example are presented in the Appendixes.

II. MODEL

Our model can broadly be divided into two primary elements. The first is the quantum dynamics described by the Schrödinger equation. The second is the measurement protocol, which yields the well-defined meaning for the position of the particle. Beginning with a description of the first part, we consider a single particle whose time evolution is described by a time-independent Hermitian Hamiltonian H according to the Schrödinger equation $H|\psi\rangle = i\hbar\frac{d}{dt}|\psi\rangle$, where we set $\hbar = 1$. The initial wave function is denoted $|\psi_{\text{in}}\rangle$. The H is represented here with a graph where nodes describe states and edges describe the hopping amplitudes between these states. Our main focus considers an H that is described by some adjacency matrix, though the theory presented below is more general.

The Hilbert space we consider is discrete and is spanned by X, which is the set of eigenvectors of the operator $\hat{X}$. $\hat{X}$ can be any arbitrary Hermitian operator as long as all of its eigenvalues are nondegenerate. In practice, in this paper, we will assume that it is the position operator for the sake of simplicity. The initial wave function $|\psi_{\text{in}}\rangle$ is localized to a single site in this space, $|\psi_{\text{in}}\rangle \in X$. For example, we consider the tight-binding infinite line lattice Hamiltonian,

$$H = -\gamma \sum_{x=-\infty}^{\infty} (|x\rangle\langle x+1| + |x+1\rangle\langle x|), \tag{1}$$

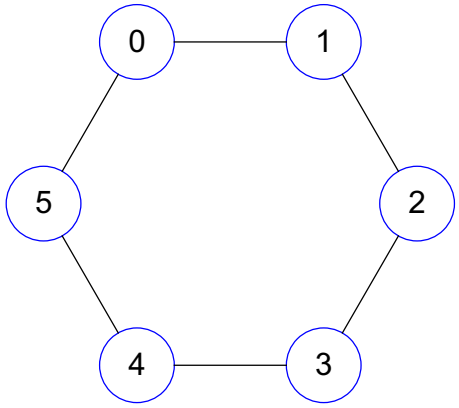

FIG. 2. Schematic model of a benzene ring. The edges represent jumps between nearest neighbors, all with the same amplitude. In Sec. VII we examine the properties of a measurement-induced quantum walk on this graph, as well as the first detection problem.

where $|\psi_{\text{in}}\rangle = |0\rangle$. This Hamiltonian describes hops between nearest neighbors on the infinite line with an amplitude γ for the jumps, and hence for an initial condition set at the origin these dynamics are sometimes called a tight-binding quantum walk [22]. In this example, the space X is defined with the vertices on the lattice $|x\rangle$, and as usual $\hat{X}|x\rangle = x|x\rangle$. A schematic representation of this Hamiltonian is given in Fig. 1. Another example is presented in Fig. 2, where we have a finite ring. It is well known that the statistical properties of first detection time for finite and infinite systems differ dramatically [8,19,23,24], so we will use these two models as examples later in Secs. VII and VIII.

To establish the position of the particle at every step of the random walk, we start by defining the measurement protocol as follows: Position measurements are performed at discrete times $t = \tau, 2\tau, \dots, N\tau$ using the position operator $\hat{X}$. Between each measurement event the dynamics are unitary, as described above. At every measurement, we obtain the exact position of the particle causing the wave function to collapse and be localized to that point on the graph. Of course, the basic postulates of quantum mechanics mean that the outcome of the measurement is random. Over the course of many measurements, this process produces a list of the locations at which the particle was detected. As the measurements combined with the unitary time evolution given by the Schrödinger equation act as the generators of this random walk, we shall henceforth refer to this process as a measurement-induced quantum walk. As an example of a particular instance of this measurement-induced quantum walk, on the infinite line Hamiltonian in Eq. (1) the eigenvalues of the position operator are the integers $X = \mathbb{Z}$, so for a walk whose initial state is the origin ($|\psi_{\text{in}}\rangle = |0\rangle$), one possible sequence of measurement outcomes is $\{x_1 = 1, x_2 = 3, x_3 = 1, x_4 = -1, x_5 = \cdots\}$. For a more general measurement-induced quantum walk, the unitary time evolution followed by measurement-induced wave function collapse repeats indefinitely, as is shown in Fig. 3.

To be more precise concerning the exact mechanics of the measurement-induced quantum walk, consider the first measurement, which occurs at $t = \tau$. Immediately before this

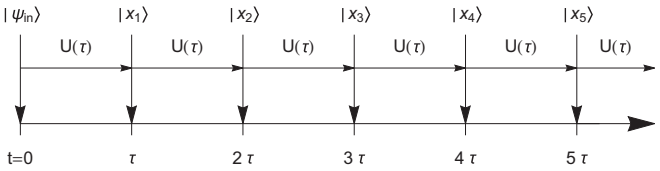

FIG. 3. A measurement-induced quantum walk that begins at $|\psi(t=0)\rangle = |\psi_{\text{in}}\rangle$. At every step of the walk, the particle is detected at some point on the graph, $|x_n\rangle$, and between each detection the wave function evolves according to the Schrödinger equation with the standard unitary time evolution operator $U(\tau) = e^{-i\tau H}$. This process can, in principle, continue indefinitely.

time at $\tau^- = \tau - \epsilon(\epsilon \to 0)$, the wave function is given by

$$|\psi(\tau^-)\rangle = e^{-i\tau^- H}\,|\psi_{\text{in}}\rangle\,. \tag{2}$$

According to the standard interpretation of measurement in quantum mechanics, the detection probability at $t = \tau$ at every graph site x is given by

$$P_1 = |\,\langle x|\psi(\tau^-)\rangle\,|^2. \tag{3}$$

After the measurement, the particle will be localized to some site which we will label as x_1. This means that at time $\tau^+ = \tau + \epsilon$, the wave function is given by

$$|\psi(\tau^+)\rangle = |x_1\rangle\,. \tag{4}$$

We then allow the system to freely evolve in time until $2\tau^- = 2\tau - \epsilon$ when it is $|\psi(2\tau^-)\rangle = e^{-i\tau^- H}\,|x_1\rangle$. We then measure the particle again, and the probability of detection for each site x is given by

$$P_2 = |\,\langle x|\psi(2\tau^-)\rangle\,|^2. \tag{5}$$

The particle is then localized to a new state, which we will label as x_2. We continue to evolve the wave function and measure its position in this manner, obtaining a list of its positions in the process $\{x_1, x_2, x_3, \ldots\}$, which we treat as being the positions that the particle traveled through over the course of its random walk.

III. DYNAMICS WITH MEASUREMENTS

The probability of detecting the particle at the state x at time τn is given by the sum of the probabilities of all paths that begin at the origin ψ_{in} and reach x after n steps. To find these probabilities, we define a vector that we will call the probability vector, which will contain the probabilities of the possible outcomes of the measurements at times that are integer multiples of τ plus an infinitesimally small positive ϵ. Since this vector is just the main diagonal of the density matrix describing the system, we will denote it as $|\rho(\tau n)\rangle$. It is a non-negative vector whose dimension is the same as that of the Hilbert space, but it is certainly not part of the Hilbert space. Since the total probability that the particle will be found somewhere on the graph is unity, the sum of the elements of the probability vector equals 1.

At time $t = 0$, we define the probability vector to equal $|\psi_{\text{in}}\rangle$, and we assume that it is an eigenstate of $\hat{X}$. In the context of tight-binding walks on a graph, this means that the system is initially localized to a node of the graph that we call

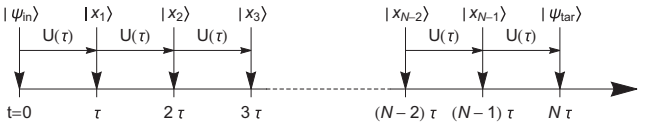

FIG. 4. A measurement-induced quantum walk which begins at $|\psi(t=0)\rangle = |\psi_{\text{in}}\rangle$ and ends after time $t = N\tau$ when the particle is detected at $|\psi_{\text{tar}}\rangle$. The underlying physical process is the same as the one that was described in Fig. 3, but in this process we stop the random walk once it is detected at the target state $|\psi_{\text{tar}}\rangle$.

$|\psi_{\text{in}}\rangle$. We address the case in which it is not initially localized in Appendix C. For the time evolution of $|\rho(\tau n)\rangle$ we define the operator G such that it will contain the probabilities for the particle to jump from any position in the system to any other position:

$$G = \sum_{x,x' \in X} |\,\langle x'|e^{-i\tau H}|x\rangle\,|^2\,|x'\rangle\,\langle x|\,. \tag{6}$$

G is a stochastic matrix, meaning that it is used to describe the transitions of a Markov chain. All of G's eigenvalues are real and have an absolute value less than or equal to 1, as is shown in Appendix B. Evolving the system in time using this matrix, the state of the system at time $t = \tau n$ is described by the probability vector

$$|\rho(\tau n)\rangle = G^n\,|\psi_{\text{in}}\rangle\,. \tag{7}$$

This is a kind of discrete-time Master equation that takes into consideration both the unitary time evolution and the periodic measurements that collapse the wave function.

In addition to the measurement-induced quantum walk itself, another topic of interest we study in this paper is the first detection problem, wherein rather than simply allowing the system to continue evolving in time indefinitely, we define a target state $|\psi_{\text{tar}}\rangle$ and we stop the random walk once the particle is detected in this state. This state can either be the same as the origin, in which case the random walk is referred to as a return problem, or it can be any other state on the graph, in which case we refer to it as a transition problem. The first hitting time is $N\tau$, and it is a random variable whose statistical properties depend on the Hamiltonian and the particular choice of sampling interval τ. The modified process for this random walk is described in Fig. 4. To account for the fact that in this version of the measurement-induced quantum walk the experiment stops when the particle is detected at ψ_{tar}, we remove the probability that the particle was found at ψ_{tar} after every τ since the continuation of the experiment necessarily means it was not found there. This effectively removes any paths that crossed through ψ_{tar} from our ensemble since those paths would have resulted in the termination of the process. Projecting the resulting probability vector unto the target state gives us the following equation for the probability of *first* detecting the particle at the target site at time $t = \tau n$, which we denote as F_n:

$$F_n = \langle\psi_{\text{tar}}|[G(1-D)]^{n-1}G|\psi_{\text{in}}\rangle\,, \tag{8}$$

where $D = |\psi_{\text{tar}}\rangle\,\langle\psi_{\text{tar}}|$ is a projecting operator. For example, for $n = 1$, we obtain $F_1 = \langle\psi_{\text{tar}}|G|\psi_{\text{in}}\rangle$. For $n = 2$, we have $F_2 = \langle\psi_{\text{tar}}|G(1 - |\psi_{\text{tar}}\rangle\,\langle\psi_{\text{tar}}|)G|\psi_{\text{in}}\rangle$ and so on. The full

derivation of Eq. (8) is presented in Appendix A. We will now further interpret Eq. (8) using a renewal equation approach.

IV. GENERATING FUNCTION

In Appendix A 3 we show that Eq. (8) is equivalent to

$$F_n = \langle\psi_{\rm tar}|G^n|\psi_{\rm in}\rangle - \sum_{j=1}^{n-1} F_j \langle\psi_{\rm tar}|G^{n-j}|\psi_{\rm tar}\rangle . \tag{9}$$

This is a renewal equation typically found for these types of problems [8,19,23]. One may obtain a simple physical interpretation of this equation by moving the sum to the left-hand side, which gives us

$$\sum_{j=1}^{n} F_j \langle\psi_{\rm tar}|G^{n-j}|\psi_{\rm tar}\rangle = \langle\psi_{\rm tar}|G^n|\psi_{\rm in}\rangle . \tag{10}$$

In doing so, we can see that the probability of arriving at the target state after n steps $\langle\psi_{\rm tar}| G^n |\psi_{\rm in}\rangle$ (not necessarily for the first time) is the same as the probability of arriving there for the first time at some earlier point in time and then looping back to return there.

To analyze F_n, we note that Eq. (9) has a convolution structure, hence we use the Z transform, or discrete Laplace transform, which is by definition [25]

$$\widetilde{F(z)} = \sum_{n=1}^{\infty} F_n z^n. \tag{11}$$

Multiplying Eq. (9) by z^n and summing over n, we get

$$\widetilde{F(z)} = \sum_{n=1}^{\infty} \langle\psi_{\rm tar}|G^n|\psi_{\rm in}\rangle - \sum_{n=1}^{\infty}\sum_{j=1}^{n-1} F_j \langle\psi_{\rm tar}|G^{n-j}|\psi_{\rm tar}\rangle . \tag{12}$$

The second term on the right-hand side of the equation is a discrete convolution, so after evaluating the sums over n and some rearrangement, we get

$$\widetilde{F(z)} = \frac{\langle\psi_{\rm tar}|\widetilde{G(z)}|\psi_{\rm in}\rangle}{1+\langle\psi_{\rm tar}|\widetilde{G(z)}|\psi_{\rm tar}\rangle}, \tag{13}$$

where $\widetilde{G(z)} = \sum_{n=1}^{\infty} z^n G^n = zG/(1-zG)$. By rearranging the generating function, we are also able to present it in a manner that better relates it to the underlying probability vector:

$$\widetilde{F(z)} = \frac{\sum_{n=1}^{\infty} z^n \langle\psi_{\rm tar}|\rho_{\rm in}(\tau n)\rangle}{\sum_{n=0}^{\infty} z^n \langle\psi_{\rm tar}|\rho_{\rm tar}(\tau n)\rangle}, \tag{14}$$

where $|\rho_{\rm in}(0)\rangle = |\psi_{\rm in}\rangle$ and $|\rho_{\rm tar}(0)\rangle = |\psi_{\rm tar}\rangle$. In the return problem where $|\psi_{\rm in}\rangle = |\psi_{\rm tar}\rangle$, this expression can be further simplified to just

$$\widetilde{F(z)} = 1 - \frac{1}{\sum_{n=0}^{\infty} z^n \langle\psi_{in}|\rho(\tau n)\rangle}. \tag{15}$$

Using the generating function, we can calculate the first detection probabilities, the survival probability, the expected number of measurement attempts, and the variance in the number of detection attempts. We formally find that they are given by

$$F_n = \frac{1}{n!}\frac{d^n}{dz^n}\widetilde{F(z)}|_{z=0} = \frac{1}{2\pi i}\oint_C \frac{\widetilde{F(z)}}{z^{n+1}}dz, \tag{16}$$

$$P_{\rm det} = \sum_{n=1}^{\infty} F_n = \widetilde{F(1)}, \tag{17}$$

$$\langle n\rangle = \sum_{n=1}^{\infty} nF_n = \frac{d}{dz}\widetilde{F(z)}|_{z=1}, \tag{18}$$

$$\langle n^2\rangle = \sum_{n=1}^{\infty} n^2 F_n = \frac{d}{dz}\left(z\frac{d}{dz}\widetilde{F(z)}\right)|_{z=1}. \tag{19}$$

Here $P_{\rm det}$ is the total detection probability after an infinite number of measurement attempts. If $P_{\rm det}$ is 1, Eqs. (18) and (19) are the moments of the first detection event. Note that like in classical random walks, the total detection probability $P_{\rm det}$ can be less than unity [8,19,23], in which case the first and second moments can no longer be used to calculate the average and variance of the first detection event as detection is not guaranteed. They can still be used to compute the average and variance conditioned on the event that the particle is detected by dividing them by the total detection probability: Average $= \langle n\rangle / P_{\rm det}$ and Variance $= \langle n^2\rangle / P_{\rm det} - \langle n\rangle^2 / P_{\rm det}^2$.

So far, the results we have obtained seem to indicate that the measurement-induced quantum walk behaves like a regular discrete-time classical random walk where other than the fact that the transition probabilities are determined using the Schrödinger equation, the process is completely classical. By this, we mean that the basic structure of the renewal equation is classical. This classical feature is related to the repeated measurements, which help us define a discrete path on the graph that the particle took, a classical feature. While the aforementioned classical trait would seem to imply that this process is purely classical, this ignores some interesting effects that arise from the combination of the unitary time evolution of the quantum wave function with the wave-function collapse introduced by repeated measurements. First, G depends of course on $\hbar$, and in that sense it is still describing a quantum-mechanical process. But more profoundly, we find that for certain sampling rates which we label as exceptional, the statistics of the system vary drastically compared to classical behavior, and that depending on the initial and target states, certain sampling rates minimize the average time until detection, whereas for others the average diverges to infinity. Such features are different compared to classical walks on similar structures and are related to periodicity, revivals, and destructive interference of the underlying quantum dynamics. These underlying dynamics embedded in G through the unitary time evolution of the wave function $U(\tau)$ make it fundamentally different from classical transition matrices despite the superficial similarities.

V. EXPECTATION VALUES AND EXCEPTIONAL SAMPLING RATES

In this section, we derive general expressions for $P_{\rm det}$, $\langle n\rangle$, and Δn^2 in finite systems. We also observe interesting effects in these values near exceptional sampling rates, examples of

which are later shown in Sec. VII. *We define these sampling rates to be those that cause 1 to be a degenerate eigenvalue of G.* We postulate that these exceptional sampling rates satisfy $\Delta E\tau = 2\pi n$, where ΔE are the non-negative differences between pairs of the Hamiltonians eigenenergies.

A. Total detection probability

As previously mentioned in Eq. (17), the total detection probability is acquired by evaluating the generating function at $z = 1$. In this section we derive a general expression for this. Since G is a real Hermitian matrix, we can express the initial and detection sites as superpositions of its eigenstates,

$$|\psi_{\text{in}}\rangle = \sum_{\lambda}\sum_{k=1}^{g_\lambda} \langle\lambda_k|\psi_{\text{in}}\rangle\,|\lambda_k\rangle\,,$$
$$|\psi_{\text{tar}}\rangle = \sum_{\lambda}\sum_{k=1}^{g_\lambda} \langle\lambda_k|\psi_{\text{tar}}\rangle\,|\lambda_k\rangle\,, \tag{20}$$

where $G\,|\lambda_k\rangle = \lambda\,|\lambda_k\rangle$ and g_λ are the degeneracies of the eigenvalues. In addition to this general form of writing the initial and target state, we also consider the state

$$|\phi\rangle = \frac{1}{\sqrt{|X|}}\sum_{x\in X}|x\rangle\,. \tag{21}$$

This is an eigenstate of G with eigenvalue 1 at all sampling rates. By the prior definition of exceptional sampling rates, for nonexceptional sampling rates $|\phi\rangle$ is the *only* G eigenstate whose eigenvalue is 1. This state serves as a kind of a ground state under the repeated measurements. In classical processes, this would correspond to a high-temperature limit (in a Boltzmann sense) since the system is evenly populating all states. The repeated measurements drive the system to this state [26].

Returning to the subject of the derivation of a general formula for P_{det}, we plug Eq. (20) into Eq. (13) to obtain

$$\widetilde{F(z)} = \frac{\sum_\lambda\sum_{k=1}^{g_\lambda}\frac{\langle\psi_{\text{tar}}|\lambda_k\rangle\langle\lambda_k|\psi_{\text{in}}\rangle z}{1-\lambda z}}{1+\sum_\lambda\sum_{k=1}^{g_\lambda}\frac{|\langle\lambda_k|\psi_{\text{tar}}\rangle|^2\lambda z}{1-\lambda z}}. \tag{22}$$

Using Eq. (17), we take the limit $z \to 1$, all of the eigenstates whose eigenvalues are less than 1 disappear, and we are left with

$$P_{\text{det}} = \widetilde{F(1)} = \frac{\sum_{k=1}^{g_1}\langle\psi_{\text{tar}}|1_k\rangle\,\langle 1_k|\psi_{\text{in}}\rangle}{\sum_{k=1}^{g_1}|\,\langle 1_k|\psi_{\text{tar}}\rangle\,|^2}, \tag{23}$$

where the summation is only over the set of eigenstates whose eigenvalue is 1, $G\,|1_k\rangle = |1_k\rangle$. This equation is general and valid for all sampling rates.

We can see from this expression that in the return problem, where we set $\langle\psi_{\text{in}}|\psi_{\text{tar}}\rangle = 1$, the total detection probability P_{det} is always 1 in a finite system. We can also see that for nonexceptional sampling rates, i.e., sampling frequencies where 1 is a nondegenerate eigenvalue of G, i.e., $g_1 = 1$, P_{det} is 1 for the transition problem as well in finite systems, since in that case the only eigenstate which will go into the sum in Eq. (23) is the uniform state given in Eq. (21). Thus, for nonexceptional sampling rates, the total detection probability is unity just like a regular classical random walk on a finite graph. This is very different from the case in which we only measure locally at the target site, where due to destructive interference we may get $P_{\text{det}} < 1$ [27–29]. We address this subject and the more general comparison between global and local measurements in Sec. IX.

B. The mean and variance in the return problem

The mean $\langle n\rangle$ for a measurement-induced quantum walk on a finite graph is the average number of attempts needed until the particle is first found at the state $|\psi_{\text{tar}}\rangle$. It is equal to the average time from the beginning of the walk until the particle is detected at the target state, divided by the time between measurements τ. Similarly to the derivation of Eq. (23), we express the initial and detection site as superpositions of G's eigenstates, plug those into Eq. (18), and take the limit as $z \to 1$ to find that in the return problem $\langle\psi_{\text{in}}|\psi_{\text{tar}}\rangle = 1$ this average is

$$\langle n\rangle = \frac{1}{\sum_{k=1}^{g_1}|\,\langle\psi_{\text{in}}|1_k\rangle\,|^2}. \tag{24}$$

For nonexceptional sampling rates, $|\phi\rangle$ is the only state in the sum, and we can simplify Eq. (24) to obtain

$$\langle n\rangle = |X|. \tag{25}$$

This means that the mean $\langle n\rangle$ is quantized and independent of the details of the system besides the dimension of the Hilbert space. Namely, recall that for any tight-binding walk on a graph X is the set of vertexes, and $|X|$ is the number of vertices.

In essence this is similar to the Kac formula for the mean, which applies for classical walks and reads $\langle n\rangle = 1/p_{\text{eq}(x)}$, where $p_{\text{eq}(x)}$ is the equilibrium state and x is the vertex [30]. However, what is remarkable here is that the effective steady state is uniform (like a high-temperature limit in classical statistical mechanics), so the corresponding equilibrium measure is $1/|X|$. Under the condition that $g_1 = 1$, we can interpret the resulting Eq. (25) as the measurements driving the system to a high-temperature classical limit [26].

One exceptional sampling rate that we can see in all systems is the Zeno limit ($\tau \to 0$). In this limit of Eq. (24), G becomes the identity matrix, which causes the sum in the divisor to evaluate to 1, and we get $\langle n\rangle = 1$. This is expected if we start at the target node and immediately measure the particle in the first attempt. What is remarkable is that if τ is very small but finite, we still get $\langle n\rangle = |X|$. So close to the Zeno limit we get a drastic jump in $\langle n\rangle$ when plotted as a function of τ. This means that the fluctuations of the first detection time $N\tau$ close to this limit are gigantic. We can also see these fluctuations in that the variance Δn^2 diverges at this limit as shown in Eq. (26). This nonanalytical behavior is also found for other exceptional sampling times, discussed below.

To find the variance in the number of measurements $\Delta n^2 = \langle n^2\rangle - \langle n\rangle^2$, we repeat the aforementioned process for Eq. (19) and find that for nonexceptional sampling rates, the variance of the number of measurements in a finite system is given by

$$\Delta n^2 = |X|^2 - |X| + 2|X|^2\sum_{\lambda\neq 1}\sum_{k=1}^{g_\lambda}|\,\langle\psi_{\text{in}}|\lambda_k\rangle\,|^2\frac{\lambda}{1-\lambda}. \tag{26}$$

We see here that as any of G's eigenvalues λ approach 1, such as in the Zeno limit, the variance diverges, which is indicative of the large fluctuations in the first detection probability, which are observed near exceptional sampling rates. Keep in mind that Eqs. (24) and (26) are only valid in the return problem $\langle\psi_{\text{in}}|\psi_{\text{tar}}\rangle = 1$. In Appendix H we present the full derivation of these two equations in detail, as well as a more general form of the equation for Δn^2, which also works for exceptional sampling rates.

Note that the quantization of the mean return time, Eq. (25), is not unique to the protocol under study. In Sec. IX we discuss other measurement schemes that yield quantization of the mean return time.

C. The mean in the transition problem

We now turn our attention to the transition problem. Similarly to the previous derivation of Eq. (24), we plug Eq. (22) into Eq. (18). After simplifying, we arrive at the following equation for $\langle n\rangle$ in the transition problem:

$$\langle n\rangle = \frac{\sum_{k=1}^{g_1}\langle\psi_{\text{tar}}|1_k\rangle\langle 1_k|\psi_{\text{in}}\rangle}{\left(\sum_{k=1}^{g_1}|\langle\psi_{\text{tar}}|1_k\rangle|^2\right)^2} + \frac{\lim_{z\to 1} g(z)}{\left(\sum_{k=1}^{g_1}|\langle\psi_{\text{tar}}|1_k\rangle|^2\right)^2}. \tag{27}$$

The function $g(z)$ is

$$g(z) = \sum_{\lambda}\sum_{k=1}^{g_\lambda}\sum_{j=1}^{g_1}\frac{\lambda z}{1-\lambda z} f(|\lambda_k\rangle, |1_j\rangle),$$

$$f(|\lambda_k\rangle, |1_j\rangle) = \langle\psi_{\text{tar}}|1_j\rangle\langle 1_j|\psi_{\text{in}}\rangle|\langle\psi_{\text{tar}}|\lambda_k\rangle|^2 - \langle\psi_{\text{tar}}|\lambda_k\rangle\langle\lambda_k|\psi_{\text{in}}\rangle|\langle\psi_{\text{tar}}|1_j\rangle|^2, \tag{28}$$

where the sums in Eq. (27) are all only over eigenstates whose eigenvalue is 1 and $G|1_j\rangle = |1_j\rangle$. In $g(z)$, the summation over λ_k includes all of G's eigenstates, whereas the sum over j is over only the eigenvectors whose eigenvalue is 1. For nonexceptional sampling rates, the sum over j is just $|\phi\rangle$, and since $\forall x \in X : f(|x\rangle, |x\rangle) = 0$, Eq. (27) reduces to

$$\langle n\rangle = |X|\left[1 + \sum_{\lambda\neq 1}\sum_{k=1}^{g_\lambda}\frac{\lambda}{1-\lambda}(|\langle\psi_{\text{tar}}|\lambda_k\rangle|^2 - \langle\psi_{\text{tar}}|\lambda_k\rangle\langle\lambda_k|\psi_{\text{in}}\rangle)\right]. \tag{29}$$

If $\lambda \to 1$, $\langle n\rangle$ can diverge. However, it should be noted that $\langle n\rangle$ does not necessarily diverge close to exceptional sampling rates since the expression in the inner brackets can equal zero. If it does not diverge, it often jumps discontinuously to a different finite value. We address this issue in Appendix D. It should also be noted that if $|\psi_{\text{in}}\rangle = |\psi_{\text{tar}}\rangle$, the sum reduces to zero and we get Eq. (25), since it is just a special case of this equation.

VI. SLOW RELAXATION OF THE SURVIVAL PROBABILITY NEAR EXCEPTIONAL SAMPLING RATES

In Sec. V we already showed that in finite systems, as the number of measurements goes to infinity, the total detection probability P_{det} converges to 1 for nonexceptional sampling rates. In this section, we show that this relaxation is considerably slower for sampling rates that are close to exceptional ones.

Starting with Eq. (8), we will define a new operator $G_{\text{tar}} = G(\mathbb{1} - |\psi_{\text{tar}}\rangle\langle\psi_{\text{tar}}|)$ and rewrite the formula with it:

$$F_n = \langle\psi_{\text{tar}}|G_{\text{tar}}^{n-1}G|\psi_{\text{in}}\rangle. \tag{30}$$

This new operator is non-Hermitian, but much like the original G all of its eigenvalues are real and less than or equal to 1. Similarly to the way we used G's eigenbasis, we will expand the initial probability vector $G|\psi_{\text{in}}\rangle$ using G_{tar}'s eigenbasis. We will denote G_{tar}'s eigenvalues as μ and its right and left eigenstates as $|\mu_R\rangle$ and $\langle\mu_L|$, where $G_{\text{tar}}|\mu_R\rangle = \mu|\mu_R\rangle$ and $\langle\mu_L|G_{\text{tar}} = \langle\mu_L|\mu$; as usual, the left and right eigenvectors have the same eigenvalues [31]. With these, we can express the first detection probability like what we did in Eq. (20), with a minor complication made by the fact that rather than span $|\psi_{\text{in}}\rangle$ using this eigenbasis, we need to span $G|\psi_{\text{in}}\rangle$ instead, where we assume that G_{tar} has no degeneracies. The aforementioned expansion gives us an equation for the first detection probability:

$$F_n = \sum_{\mu}\mu^{n-1}\frac{\langle\mu_L|G|\psi_{\text{in}}\rangle}{\langle\mu_L|\mu_R\rangle}\langle\psi_{\text{tar}}|\mu_R\rangle. \tag{31}$$

Equation (31) is a formal solution of the problem. It shows that F_n decays exponentially as a function of n provided that the sampling rate is nonexceptional.

Using Eq. (31) and the insight from Eq. (23) that the total detection probability for nonexceptional sampling rates is 1, we can derive the following equation for the survival probability $S_N = 1 - \sum_{j=1}^{N}F_j$, which is the probability that in a finite system the particle was not detected, namely that it survived. We find

$$S_N = \sum_{\mu}\frac{e^{N\ln\mu}}{1-\mu}\frac{\langle\mu_L|G|\psi_{\text{in}}\rangle}{\langle\mu_L|\mu_R\rangle}\langle\psi_{\text{tar}}|\mu_R\rangle. \tag{32}$$

Based on this equation, we can see that we should expect the survival probability to exponentially decay to zero for nonexceptional sampling rates and that the decay rate should slow down considerably when one or more of G_{tar}'s eigenvalues approaches 1 since the decay rates are given by $\ln\mu$. As we will now show using an interlacing technique [32], this happens close to every exceptional sampling rate.

To see this, we first note that G_{tar}'s eigenvalues satisfy the equation

$$\text{Eigenvalues}(G_{\text{tar}}) = \{0\} \cup \text{Eigenvalues}(G'), \tag{33}$$

where G' is the principal submatrix of G, where the row and column corresponding to ψ_{tar} have been removed. Note that G' is Hermitian and also a principal submatrix of G_{tar}. This is significant thanks to the Cauchy Interlace Theorem [33], which states the following:

For any pair of Hermitian matrices A and B of order N and $N-1$, respectively, where B is a principal submatrix of A, the eigenvalues of the two matrices interlace. This means that if we label A's eigenvalues as a_n such that $a_{n-1} \leqslant a_n$ and label

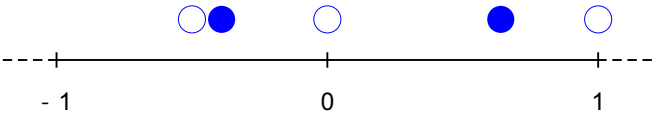

FIG. 5. A simple illustration of the eigenvalue interlacing theorem. The eigenvalues of G and G' for the Hamiltonian (35) plotted on a segment of the real number line. G's eigenvalues are depicted as blue circles, whereas the eigenvalues of G' are depicted as blue disks. We find that the eigenvalues of G' always interlace between G's eigenvalues just as the theorem predicts.

B's eigenvalues as b_n such that $b_{n-1} \leqslant b_n$, then

$$a_1 \leqslant b_1 \leqslant a_2 \leqslant b_2 \leqslant \cdots \leqslant b_{N-2} \leqslant a_{N-1} \leqslant b_{N-1} \leqslant a_N. \tag{34}$$

To show how this affects our problem using an example we examine a transition from $|0\rangle$ to $|2\rangle$ on a simple three-site line graph, which is described by the following tight-binding Hamiltonian:

$$H = -\gamma(|0\rangle\langle 1| + |1\rangle\langle 0| + |1\rangle\langle 2| + |2\rangle\langle 1|). \tag{35}$$

After using Eq. (6) to find G and G', we evaluate them at the nonexceptional sampling rate $\gamma\tau = \pi/\sqrt{8}$ and then calculate their eigenvalues. We find that the eigenvalues of the two matrices interlace just like the theorem predicts, as is shown in Fig. 5.

Except for zero, which is always an eigenvalue of G_{tar}, this interlacing occurs for all values of $\gamma\tau$, meaning that there is always a μ between every pair of λ's. As τ approaches an exceptional sampling rate, one of G's eigenvalues will approach unity. Since $\lambda = 1$ is always an eigenvalue of G, the μ that is interlaced between it and the aforementioned eigenvalue must also coalesce on unity as it is squeezed between the two G eigenvalues. This causes the survival probability decay to slow down considerably since, as mentioned in Eq. (32), $\mu \to 1$ implies slow relaxation. To show this, we plot the eigenvalues of G and G_{tar} together as a function of $\gamma\tau$ in Fig. 6. We can see that near every exceptional sampling point, as one of G's eigenvalues approaches 1, the G_{tar} eigenvalue trapped between it and 1 is forced to also converge to 1 to preserve the interlacing property.

To see how this affects the survival probability, we plot it as a function of N for the two almost exceptional sampling rates $\gamma\tau = \epsilon$ and $\pi/\sqrt{2} - \epsilon$, where $\epsilon = 10^{-1}$. We also plot along side them the survival probability for the nonexceptional sampling rate $\gamma\tau = \pi/\sqrt{8}$ for comparison. As can be seen in Fig. 7, the decay rate is considerably slower for the two almost exceptional sampling rates compared to the nonexceptional one. To summarize, the slow decay of the survival probability near-certain sampling rates can be understood using the eigenvalue interlacing theorem. We do this by searching for sampling rates that cause an eigenvalue of G to approach unity (besides $|\phi\rangle$'s eigenvalue, which is always 1). In general, this can be done using any parameter of the Hamiltonian, not just the sampling rate. This in turn implies that an eigenvalue μ will also approach unity, and hence using Eqs. (31) and (32) the relaxation rate is reduced drastically unless prefactors vanish as well. This analysis using G_{tar} is in some sense redundant as we have already analyzed G. However, in examining both matrices and their properties, we can gain various insights into the behavior of the system that would be more difficult to notice in analyzing just one or the other.

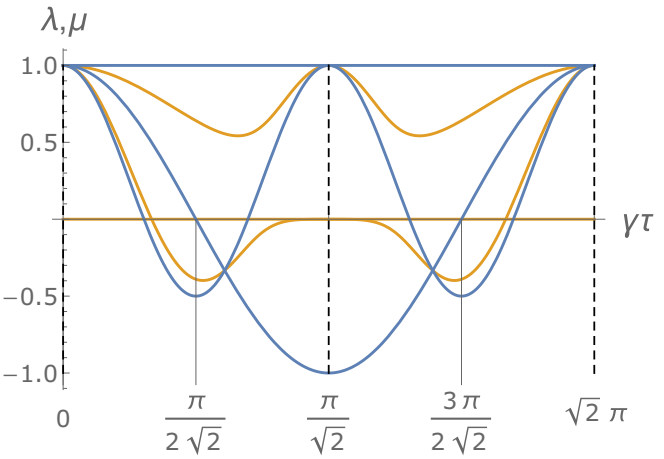

FIG. 6. The eigenvalues of G (denoted λ) and G_{tar} (denoted μ) plotted in blue and orange, respectively. For all values of $\gamma\tau$ there is always a μ between every pair of λ aside from zero which does not interlace. The eigenenergies of the system are $0, \pm\sqrt{2}\gamma$. The exceptional sampling rates are $\gamma\tau = 0, \pi/\sqrt{2}$, and $\sqrt{2}\pi$ plus integer multiples of $\sqrt{2}\pi$. In the figure these are marked by dashed lines, and all of them satisfy $\Delta E\tau = 2\pi k$. Near each of the exceptional sampling rates, we can see that at least one of the μ's is squeezed between a pair of λ's until it equals 1.

VII. BENZENELIKE RING

As an example of how our formalism can be used, we study the measurement-induced quantum walk, and we solve the return problem as well as a transition problem for a six-site

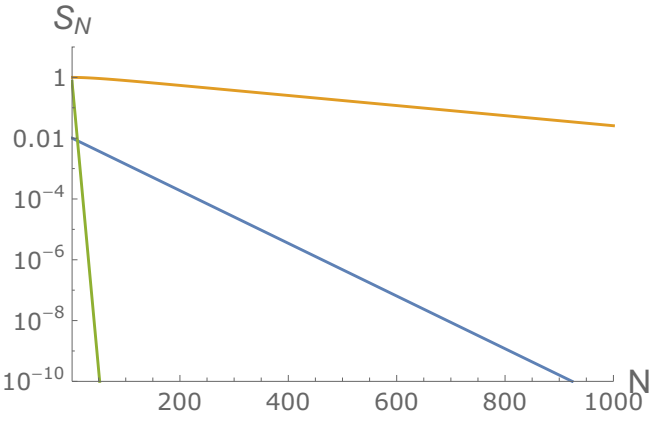

FIG. 7. The survival probability in the transition from $|0\rangle$ to $|2\rangle$ on the graph whose Hamiltonian is described in Eq. (35). The orange and blue lines correspond to the almost exceptional sampling rates $\gamma\tau = \epsilon$ and $\pi/\sqrt{2} + \epsilon$, where $\epsilon = 10^{-1}$. The green line corresponds to the nonexceptional sampling rate $\pi/\sqrt{8}$. As explained in the text, the interlacing theorem predicts the slow decay of the survival probability close to the exceptional sampling rates through the analysis of the eigenvalues of G. Whenever two eigenvalues of G merge, we get a slow relaxation of the survival probability.

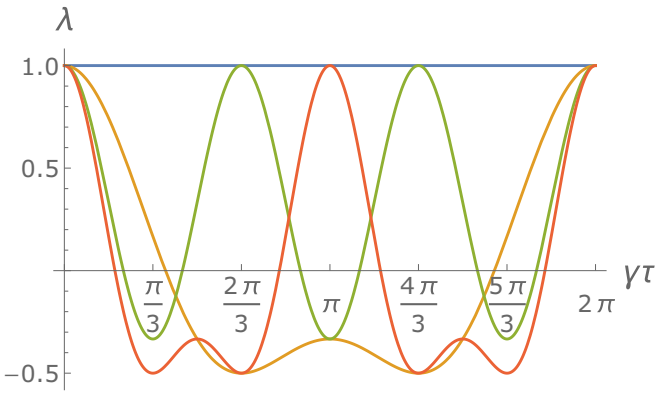

FIG. 8. The eigenvalues of G vs $\gamma\tau$ for the benzenelike ring. As with every other system, one of the eigenvalues is a constant one while the others are sinusoidal functions of $\gamma\tau$. Interesting effects that are shown in the following figures are observed when $\lambda = 1$ becomes degenerate. The exceptional sampling rates of this Hamiltonian are as follows: $\gamma\tau = 0, 2\pi/3, \pi, 4\pi/3, 2\pi$ plus every integer multiple of 2π. These sampling rates all satisfy $\Delta E\tau = 2\pi k$, where ΔE are the non-negative differences between eigenenergies of the Hamiltonian given in Eq. (36). The eigenvalues plotted in orange and green have twofold degeneracy each.

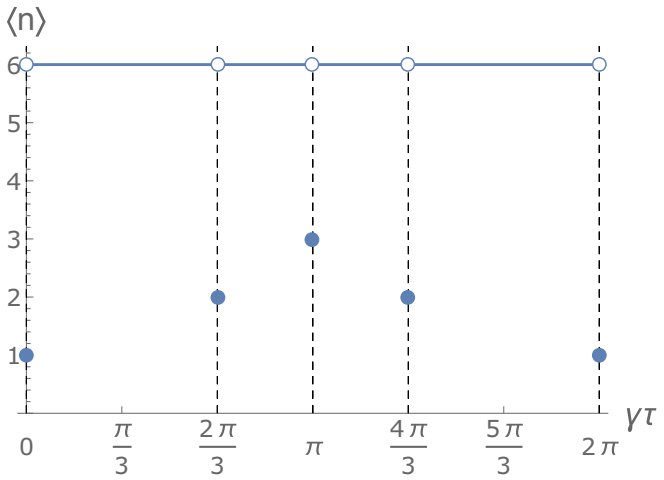

FIG. 9. $\langle n\rangle$ for the return problem for a model ring with six sites whose Hamiltonian is given by Eq. (36). As predicted by Eq. (25), $\langle n\rangle = 6$ for nonexceptional sampling rates. We find that at every exceptional sampling rate, $\langle n\rangle$ jumps discontinuously to a different integer smaller than 6. In the text we show that this happens because at those values of $\gamma\tau$ the connectivity of the graph is broken, which separates it into several fragmented graphs.

ring graph (see Fig. 2). In this solution, we omit some of the simpler steps of the process to focus instead on the results and their implications. In Appendix E we solve the first detection problem for a two-level system giving the full technical details. The graph is described by the following tight-binding Hamiltonian with cyclical boundary conditions ($|6\rangle = |0\rangle$):

$$H = -\gamma \sum_{x=0}^{5} (|x\rangle\langle x+1| + |x+1\rangle\langle x|). \tag{36}$$

We diagonalize the Hamiltonian to obtain G and then diagonalize it to obtain the eigenstates and eigenvalues, the latter of which we plot as a function of $\gamma\tau$ in Fig. 8. Having found G's eigenstates and eigenvalues, the latter of which we plotted as a function of $\gamma\tau$ in Fig. 8, we can now easily solve any measurement-induced quantum first detection problem on the hexagonal graph. Before we do that, however, we first look at the time evolution of the probability vector free of absorbing boundary conditions $|\rho(\tau n)\rangle$, which we can easily obtain using

$$|\rho(\tau n)\rangle = \sum_{\lambda} \sum_{k=1}^{g_\lambda} \lambda^n \langle\lambda_k|\psi_{\rm in}\rangle\, |\lambda_k\rangle\,. \tag{37}$$

Doing this, we find that the projection of the probability vector unto every graph site equals $1/6$ plus an exponentially decaying sum of sinusoidal functions of $\gamma\tau$, meaning that in the long time limit the system decays to the state $|\phi\rangle$ as expected. We also find that at exceptional sampling rates, some of said sinusoidal functions equal zero. We explain this phenomenon and its physical implications near the end of this section.

Returning to the topic of the first detection problem, in this section we will solve the return problem from $|\psi_{\rm in}\rangle = |0\rangle$ to $|\psi_{\rm tar}\rangle = |0\rangle$ and the transition problem from $|\psi_{\rm in}\rangle = |0\rangle$ to $|\psi_{\rm tar}\rangle = |3\rangle$. Note that the choice to examine the transition problem from $|0\rangle$ to $|3\rangle$ as opposed to other less symmetric transitions is arbitrary, and similar effects are observed for $|0\rangle$ to $|1\rangle$ and $|0\rangle$ to $|2\rangle$ as well. We briefly address the other transitions at the end of this section.

In both the return and all of the possible transitions, we find that the total detection probability $P_{\rm det}$ is 1 for nonexceptional sampling rates. In the return problem, we find that $\langle n\rangle$ is discontinuous at the exceptional sampling rates, and in the transition problem we find that it often diverges. In both, we find that the variance diverges at these sampling rates. In Figs. 9–12 we plot these values as a function of $\gamma\tau$, and we denote the exceptional values of $\gamma\tau$ with dashed vertical lines.

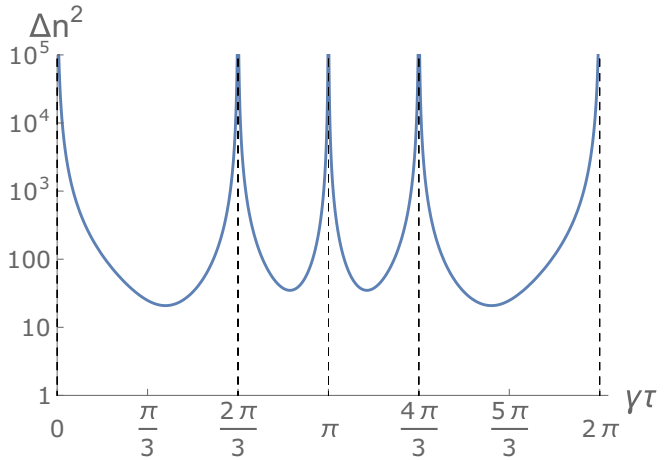

FIG. 10. $\Delta n^2 = \langle n^2\rangle - \langle n\rangle^2$ for the return problem on a model ring with six sites whose Hamiltonian is given by Eq. (36). As predicted in Eq. (26), we find that the variance diverges at every exceptional sampling rate, namely whenever a pair of λ's in Fig, 8 coalesce on unity.

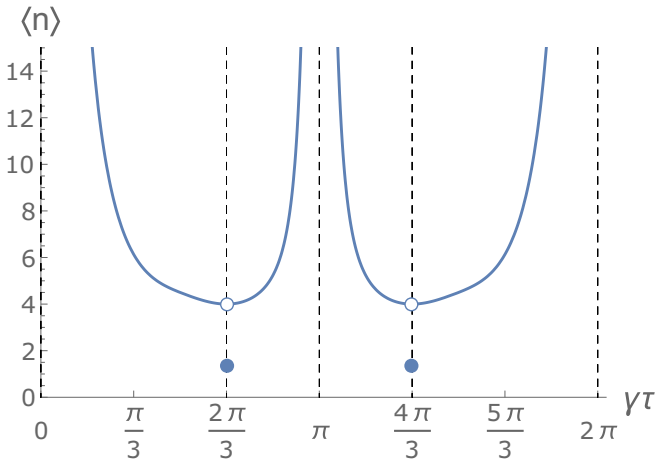

FIG. 11. $\langle n\rangle$ for the transition problem from $|\psi_{\text{in}}\rangle = |0\rangle$ to $|\psi_{\text{tar}}\rangle = |3\rangle$ on a model ring with six sites whose Hamiltonian is given by Eq. (36). In the text we explain why it diverges at $\gamma\tau = \pi n$ but only jumps discontinuously at the other sampling rates.

To better understand these discontinuities and divergences, we evaluate the stochastic matrix describing the process G at the exceptional values of $\gamma\tau$ and observe that at those points the ergodicity of the system is broken. In Fig. 13, we graph the system for various values of $\gamma\tau$ based on the G we obtain for the sampling rate. This shows us what possible transitions exist in the system at these sampling rates. We can see that the exceptional sampling rates are ones where the graph "breaks apart" into several disconnected sub-graphs, whereas for nonexceptional sampling rates every transition is possible with some nonzero probability. This effect is somewhat similar to fragmentation of the Hilbert space [27–29] and the formation of quantum many-body scars [34,35], and it results in analogous behavior of the system. Note that in Fig. 13 the lines denote nonzero transition probabilities after

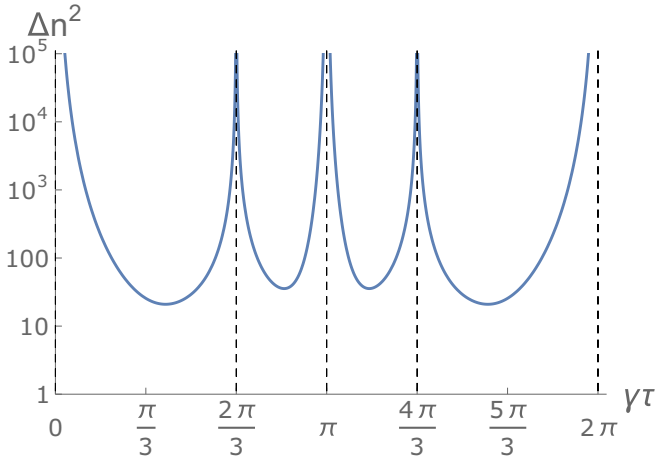

FIG. 12. $\Delta n^2 = \langle n^2\rangle - \langle n\rangle^2$ for the transition problem from $|\psi_{\text{in}}\rangle = |0\rangle$ to $|\psi_{\text{tar}}\rangle = |3\rangle$ on a model ring with six sites whose Hamiltonian is given by Eq. (36). We find that the variance diverges at every exceptional sampling rate, including $2\pi n/3$, in spite of the fact that the average does not diverge there and only jumps discontinuously.

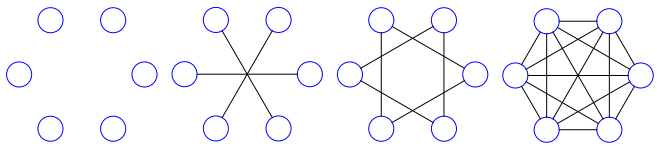

FIG. 13. The possible transitions for various sampling rates on a model ring with six sites whose Hamiltonian is given by Eq. (36). In the text we explain how this result relates to the behavior of the system, and in particular P_{det} and $\langle n\rangle$. Note that in (c), n is odd.

a measurement, unlike in Fig. 2, where the lines denoted interactions between pairs of adjacent sites. Looking at these graphs, we can also clearly see that the reason $\langle n\rangle$ in the transition problem diverged at $\gamma\tau = \pi$, but only discontinuously jumped to a different finite value at $\gamma\tau = 2\pi n/3$, is that whereas for $\gamma\tau = 2\pi n/3$ the point $|3\rangle$ remains reachable from $|0\rangle$, for $\gamma\tau = \pi n$ it becomes completely unreachable as demonstrated in Fig. 13. Using Fig. 13, we can also see that in the return problem the average is still equal to the size of the graph even for exceptional sampling rates, and the reason it jumps discontinuously from 6 to a smaller integer is that the graph itself is effectively split apart at the exceptional sampling rates. For example, for $\gamma\tau = 2\pi n$ the effective size of the graph is not 6 but rather 1 [as shown in Fig. 13(a)]. Hence for these sampling times, $\langle n\rangle = 1$ for the return problem.

Based on Fig. 13, we can also see that similar behavior will occur for other transitions. In the transition $|0\rangle$ to $|1\rangle$, $\langle n\rangle$ will diverge at every exceptional sampling rate, since $|1\rangle$ becomes unreachable at all of them, whereas in the transition from $|0\rangle$ to $|2\rangle$, $\langle n\rangle$ will diverge at $\gamma\tau = 2\pi n/3$, since $|2\rangle$ becomes unreachable at this value and it will jump discontinuously at $\gamma\tau = \pi$.

Looking back at the probability vector $|\rho(\tau n)\rangle$, we can also see that as expected at exceptional sampling rates, rather than decaying to $|\phi\rangle$, which is evenly distributed across the entire graph, it decays to an even distribution across only the subgraph to which $|\psi_{\text{in}}\rangle$ belongs.

VIII. UNBOUNDED QUANTUM WALKER IN ONE DIMENSION

In this section, we consider a measurement-induced quantum walk for a free particle on an infinite lattice. In classical random walk theory, this is the problem of first passage time for a particle diffusing without bias on a lattice in one dimension, which is of course a well-studied problem [8,23].

We use the tight-binding Hamiltonian,

$$H = -\gamma \sum_{x=-\infty}^{\infty} |x\rangle\langle x+1| + |x+1\rangle\langle x|\,. \tag{38}$$

A schematic description of this system is given in Fig. 1.

We start by first examining the behavior of the probability vector without absorbing boundary conditions, which is given by Eq. (7). The solution of the Schrödinger equation for the Hamiltonian (38) is $|\psi(t)\rangle = \sum_{x=-\infty}^{\infty} B_x |x\rangle$, where the amplitudes satisfy $i\dot{B}_x = -\gamma(B_{x+1} + B_{x-1})$. Using the Bessel function identity $2J_v'(z) = J_{v-1}(z) - J_{v+1}(z)$ [36]

and the initial condition $B_x(t=0)=\delta_{x,0}$, we find that without measurement, the wave function is

$$|\psi(t)\rangle = \sum_{x=-\infty}^{\infty} i^x J_x(2\gamma t)\,|x\rangle\,. \tag{39}$$

From this it is clear that the time evolution operator G will be

$$G = \sum_{x,x'=-\infty}^{\infty} |J_{x-x'}(2\gamma\tau)|^2\,|x\rangle\,\langle x'|\,. \tag{40}$$

Using this, we find that the Fourier transform of the probability vector at time $t=\tau n$ is given by

$$\widetilde{P}_{k,n} = \sum_k e^{-ikx}\,\langle x|\rho(\tau n)\rangle = J_0\left(4\gamma\tau\sin\left(\frac{k}{2}\right)\right)^n. \tag{41}$$

We present the exact derivation of this expression in Appendix F. We can obtain the moments of the random walk using derivatives of this Fourier transform. The first moment $\langle x\rangle$ is zero from symmetry and the second moment, which corresponds to the unitless variance in position of the random walk, is

$$\Delta x^2 = 2n\gamma^2\tau^2. \tag{42}$$

The probability vector after the first four measurements is shown for reference in Fig. 14.

A. Edgeworth series

We will start by examining the region of the random walk close to the origin. As one might expect, in this region the probability vector quickly converges to a Gaussian, which can be shown with a cumulant expansion up to the second order.

$$J_0\left(4\gamma\tau\sin\left(\frac{k}{2}\right)\right)^n \sim e^{-n\gamma^2\tau^2k^2}. \tag{43}$$

Under this simple approximation, the probability vector equals

$$\langle x|\rho(\tau n)\rangle = P_{x,n} \approx \frac{\exp\left(-\frac{x^2}{4n\gamma^2\tau^2}\right)}{\sqrt{4\pi n\gamma^2\tau^2}}. \tag{44}$$

We can reintroduce $\hbar$ to Eq. (44) and add a lattice size a, which we define to be the distance between different sites on the lattice, to get

$$P_{x,n} \approx \frac{\exp\left(-\frac{\hbar^2x^2}{4na^2\gamma^2\tau^2}\right)}{\sqrt{4\pi na^2\gamma^2\tau^2/\hbar^2}}. \tag{45}$$

To find the corrections to the Gaussian near the origin, we will use an Edgeworth series [37], which is given by

$$P_{x,n} = \frac{\exp\left(-\frac{x^2}{2c_2}\right)}{\sqrt{2\pi c_2}}\left(1+\sum_{l=2}^{\infty}\frac{(-1)^l c_{2l}}{(2l)!(2c_2)^l}H_{2l}\left(\frac{x}{\sqrt{2c_2}}\right)\right), \tag{46}$$

where $H_m(x)$ are the Hermite polynomials, and c_l is the lth cumulant of the random walk. These can be obtained using

$$c_l = i^l\lim_{k\to0}\frac{d^l}{dk^l}\ln\left(\widetilde{P}_{k,n}\right) = i^l n\lim_{k\to0}\frac{d^l}{dk^l}\ln\left(\widetilde{P}_{k,1}\right). \tag{47}$$

Since the cumulants are linearly proportional to n, the corrections to the Gaussian in Eq. (46) disappear over time, as expected. A short list of some of the cumulants is given in Table I. The Edgeworth series gives us a more accurate approximation of the probability vector near the origin than just the Gaussian, which is its first term. One way to see this is that we can retrieve the Hermite polynomials from the random

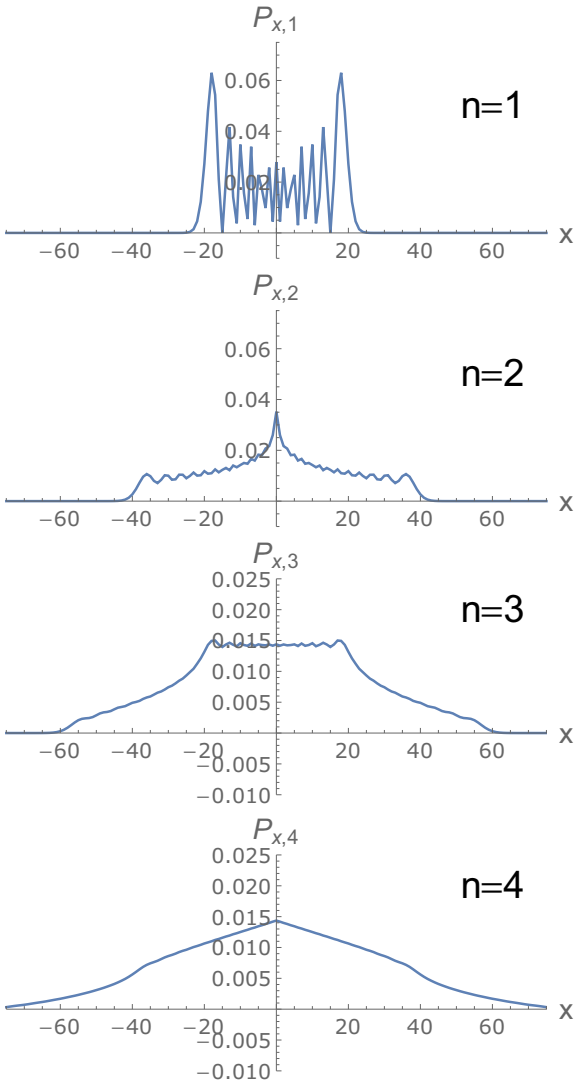

FIG. 14. The probability vector on the infinite line Hamiltonian given in Eq. (38) after the first four measurements plotted as a function of the lattice site x with $\gamma\tau=10$. The shape after the first measurement matches the results obtained in experimental implementations of this type of random walk [38], indicating that the Hamiltonian we use [Eq. (38)] can accurately model such a system. We tested many values of the sampling rate and found that excluding $\gamma\tau \ll 1$, the general shape of the distribution after the first few measurements is the one presented here. The scale of the shape depends on the sampling rate, and we find that the "width" equals $2n\gamma\tau$, as can be seen in this figure. More generally, we can say that the maximum group velocity of the wave packet when evolving without measurement is 2γ, and this is reflected here in the distance at which we can detect the particle. From the fifth measurement onward, the probability vector typically converges to a simple Gaussian shape near the center, as expected. We study the behavior of the tails of the distribution separately later in this section.

TABLE I. The first ten cumulants of the random walk on the infinite line, which are the coefficient of the series expansion of the natural log of Eq. (41) at $k = 0$. It should be noted that the special value of $\gamma\tau$, which causes the Kurtosis c_4/σ^4 to go to zero, has no particular significance with regard to the Gaussianity of the distribution, and is just coincidental.

n	c_n
0	0
2	$2n\gamma^2\tau^2$
4	$2n\gamma^2\tau^2(1-3\gamma^2\tau^2)$
6	$2n\gamma^2\tau^2(1-15\gamma^2\tau^2+40\gamma^4\tau^4)$
8	$2n\gamma^2\tau^2(1-63\gamma^2\tau^2+560\gamma^4\tau^4-1155\gamma^6\tau^6)$
10	$2n\gamma^2\tau^2(1-255\gamma^2\tau^2+5880\gamma^4\tau^4-34\,650\gamma^6\tau^6+57\,456\gamma^8\tau^8)$

walk itself. To obtain the fourth Hermite polynomial, which is the second term of the series, we can divide $P_{x,n}$ by the Gaussian term to get

$$H_4\left(\frac{x}{\sqrt{2c_2}}\right) \approx \frac{(4)!(2c_2)^2}{c_4}\left(\frac{P_{x,n}}{N_{x,n}} - 1\right), \tag{48}$$

where $N_{x,n}$ is a Gaussian (*N*ormal distribution) with $\mu = 0$ and $\sigma^2 = c_2$. In Fig. 15 we demonstrate this using a numerical simulation of the random walk.

B. Saddle point

While the Edgeworth series is useful for studying the probability vector near the origin, its accuracy decreases drastically as we move towards the tails of the distribution, to the point that it can sometimes give negative values for the probabilities. For these regions, we use a saddle point method [39] to approximate the probabilities for large values of n; full details of the derivation are given in Appendix G. While our focus with this method is the tails of this distribution, it should be noted that using it to approximate the distribution near the origin gives a Gaussian distribution as

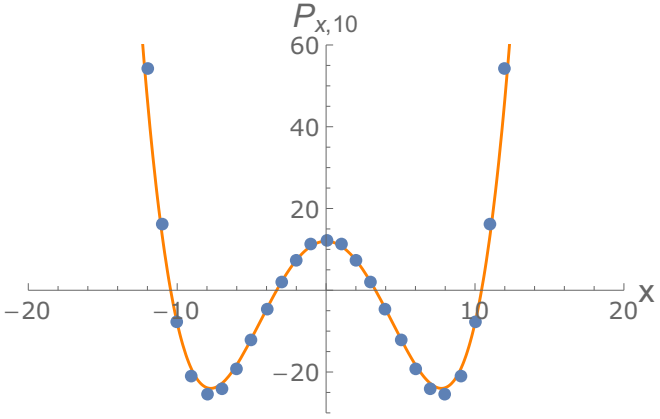

FIG. 15. A plot of the expression given in Eq. (48) for $\gamma\tau = 1$ and $n = 10$. The probabilities of detection that were obtained via numerical integration are plotted as blue dots, and the fourth Hermite polynomial is plotted as an orange line. Numerical simulations indicate that typically the two overlap almost completely for $10 \leqslant n$.

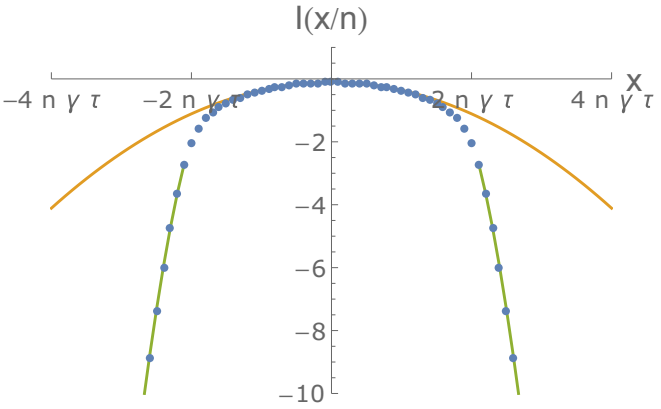

FIG. 16. The rate function $I(x/n) = n^{-1}\ln(P_{x,n})$ on the infinite 1D line plotted in blue as a function of the lattice site x. The small l approximation (Gaussian) is plotted in orange, and the large l approximation [Eq. (49)] is plotted in green. We tested many values of the sampling rate, and we found that, excluding $\gamma\tau \ll 1$, the distribution fits the Gaussian approximation up to around $|x| = 2n\gamma\tau$ and then almost immediately fits the large l approximation.

expected (Appendix G 1). For the far tails of the distribution, which we define as the region where $2n\gamma\tau \ll x$, we find in Appendix G 2 that the probabilities are given by

$$P_{x,n} \approx \frac{1}{2\pi n\gamma\tau\sqrt{\left(\frac{x}{2\gamma\tau n}\right)^2 - 1}} \frac{I_0\left(4\gamma\tau\sqrt{\left(\frac{x}{2\gamma\tau n}\right)^2 - 1}\right)^n}{\exp\left[2x\,\mathrm{arccosh}\left(\frac{x}{2\gamma\tau n}\right)\right]}, \tag{49}$$

where $I_0(x)$ is the zeroth modified Bessel function of the first kind. In the region after $x = 2n\gamma\tau$, we find that the probabilities decay rapidly, much faster than a Gaussian, as shown in Fig. 16.

C. Zeno limit

Another topic of interest in this random walk is the Zeno limit, where we take $\tau \to 0$. We can gain some simple insight into the behavior of the probability vector in this limit by taking the limit of G, which gives us

$$G \approx \sum_{x=-\infty}^{\infty} (1 - 2\gamma^2\tau^2)\,|x\rangle\langle x| + \gamma^2\tau^2(|x+1\rangle\langle x| + |x\rangle\langle x+1|). \tag{50}$$

Since the prefactors of the probability of transition are quadratic in τ, even if we consider the actual time $t = \tau n$ as opposed to the number of steps, the particle is still forced to remain at the origin and has a very low probability of escaping. Another way of seeing this is that the diffusion coefficient of this random walk is proportional to τ^2. We can better quantify this effect by examining the Kurtosis of the probability vector. The Kurtosis is a measure of the Gaussianity of the system, it is zero for Gaussian distributions and expected to be small for distributions that are very similar to Gaussians. In our previous discussion of the Edgeworth series, we mentioned that we expect the probability vector to converge to a Gaussian fairly quickly, and using the Kurtosis, we can quantify how

TABLE II. The first five first detection probabilities for the return problem on the infinite line lattice. In this table, we denoted $(2\pi)^{-1}\int_0^{2\pi}(J_0(4\gamma\tau\sin(k/2)))^n dk$ as A_n for the sake of readability.

n	F_n
1	$A_1 = \lvert J_0(2\gamma\tau)\rvert^2$
2	$A_2 - A_1^2$
3	$A_3 - A_1A_2 + A_1^3$
4	$A_4 + 3A_1^2A_2 - 2A_1A_3 - A_2^2 - A_1^4$
5	$A_5 + 3A_1^2A_3 + 3A_1A_2^2 - 2A_1A_4 - 4A_1^3A_2 - 2A_2A_3 + A_1^5$

quickly this happens. The Kurtosis for this random walk is

$$\kappa = \frac{c_4}{(c_2)^2} = \frac{(\gamma\tau)^{-2} - 3}{2n} \approx \frac{(\gamma\tau)^{-2}}{2n} \tag{51}$$

(the -3 is negligible in the Zeno limit). To obtain a Kurtosis smaller than ϵ where $\epsilon \ll 1$, we can rearrange Eq. (51) to get

$$\tfrac{1}{2}\epsilon^{-1} \leqslant n(\gamma\tau)^2, \tag{52}$$

meaning that n must be at least of the order of $(\gamma\tau)^{-2}$ for the probability vector to converge to a Gaussian shape.

D. First detection time

Turning our attention to the first detection time for the return problem on this lattice, we can easily obtain the generating function by plugging the inverse Fourier transform of Eq. (41) into Eq. (15) and perform the summation with respect to n to get

$$\widetilde{F(z)} = 1 - \frac{2\pi}{\int_0^{2\pi} \frac{dk}{1 - zJ_0\left[4\gamma\tau\sin\left(\frac{k}{2}\right)\right]}}. \tag{53}$$

Since the integral in Eq. (53) diverges for $z \to 1$, using Eq. (17) we know that for all τ, $P_{\rm det} = 1$. The small n first detection probabilities can be obtained using Eq. (9) or Eq. (16) by expanding Eq. (53) around $z = 0$ and numerically solving the resulting integrals. The exact form of the first few of these is presented in Table II. We can also continue with such a process with a program like MATHEMATICA to obtain F_n, which we plot versus n in Fig. 17.

To obtain the asymptotic behavior of the probabilities for large n we can solve the integral in Eq. (53) in the limit $1 - z \ll 1$. In this limit, most of the contribution to the integral is in the region of $k = 0$, so we will expand the Bessel function around this point up to the second-order $J_0[4\gamma\tau\sin(k)] \approx 1 - 4\gamma^2\tau^2k^2$. This approximation is accurate in the region that contributes the most to the integral and quickly decays to zero in the region that by comparison contributes very little.

With this approximation, we obtain

$$\widetilde{F(z)} \approx 1 - 2\gamma\tau\sqrt{1 - z}. \tag{54}$$

From the expansion of the function about $z = 1$ using the Tauberian theorem [8], we can see that the asymptotic big n behavior is

$$F_{1 \ll n} \approx \pi^{-1/2}\gamma\tau n^{-3/2}. \tag{55}$$

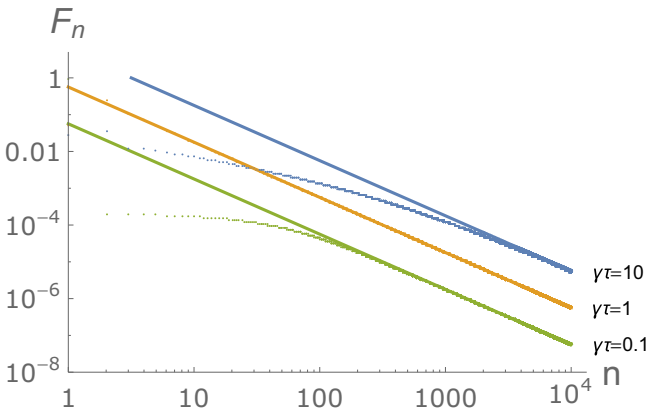

FIG. 17. F_n of the return problem on the infinite 1D line for various values of $\gamma\tau$ plotted as dots alongside their respective asymptotic limits, which were plotted as lines. The choice of sampling rate has a strong effect on the first few first detection probabilities, but after those, they all converge to $\pi^{-0.5}\gamma\tau n^{-3/2}$. This convergence is generally faster for smaller values of $\gamma\tau$, but it slows down close to the Zeno limit.

The asymptotic $n^{-3/2}$ behavior is of course similar to the well-known result from one-dimensional first passage times (classical) on a line [8,23]. We show the convergence of the first detection probabilities to this limit in Fig. 17. The prefactor we find here is the new element of this research.

In addition to the example we have considered here, an examination of the effects of Anderson localization on this kind of random walk would be interesting, as the combination of the localization caused by the measurements with the localization of the Hamiltonian eigenstates caused by disorder in the lattice might result in unique effects.

IX. COMPARISON WITH TARGET SITE MEASUREMENT

One last subject to consider is alternate definitions for a quantum first detection problem. In this paper, we considered a quantum first detection problem where every τ time we measure the position of the particle until it reaches the target site. One other possible definition of a quantum first detection problem is one where every τ time we just measure if the particle reached the target site or not using the projection operator $\lvert\psi_{\rm tar}\rangle\langle\psi_{\rm tar}\rvert$ as opposed to the position operator $\hat{X}$. This issue was considered in [19–21]. In the latter case, the outcome of each measurement is either yes or no, hence we can claim that the measurement is local. The basic renewal equations—Eq. (9) here and Eq. (17) in [19]—are fundamentally different, as here we describe a probability F_n and the latter describes an amplitude of first detection. In the classical world, the two protocols give the same first passage time statistics, but in quantum mechanics this is not the case. The current problem is more classical, but some traces of quantum mechanics are still present in the features of G, such as the exceptional sampling rates, the Zeno limit, etc.

For a more quantitative examination, we compare some of the general results obtained for both measurement protocols to highlight the differences between the two. Of particular interest are $P_{\rm det}$ and $\langle n\rangle$ for a finite Hilbert space, since we

have general results for both in both measurement protocols that apply for all time-independent Hamiltonians at nonexceptional sampling rates. Note that in general the exceptional sampling rates in the position measurement protocol and the target site measurement protocol are different, though some can be the same (such as the Zeno limit, which exists in every system and for both protocols).

For the return problem, we found in this paper that the total detection probability is always 1. This is similar to the case when measurements are performed only at the target site, which in this case is also the initial location of the wave function. The total detection probability is 1 in a finite Hilbert space with a discrete energy spectrum [14]. We found that $\langle n\rangle$ equals the size of the graph in our measurement protocol, whereas when only measuring at the target site, it was found that $\langle n\rangle$ equals the effective dimension of the Hilbert space, which is the number of distinct energy levels of the system, provided that the corresponding eigenstates have a nonzero overlap with the detected state. This effective dimension is always less than or equal to the size of the graph, so the target site measurement protocol results in faster detection on average. Note that this is true typically in ordered systems where we have some symmetry and hence degeneracy in the energy levels, whereas in disordered systems the number of energy levels is typically the same as the dimension of the Hilbert space, causing the two averages to be the same. Similar results are found also for non-Hermitian descriptions of the system [40].

For the transition problem, we found in this paper that the total detection probability is also always 1, whereas for the target site measurement protocol $P_{\rm det}$ can be bounded numbers smaller than unity depending on the symmetry of the system, as was shown in [27–29]. In general, for systems with symmetry, the repeated local measurements yield states that are called dark states [27–29], and here we did not find such generic states (except for the exceptional sampling rates, which are related to the stroboscopic protocol under study).

Although comparing $\langle n\rangle$ in the transition problem is not as easy, as we do not have a simple way of determining which measurement scheme is slower on average for it in general, we feel that the probability of not detecting the particle at all in the target site measurement scheme makes the location measurement scheme preferable for reliable detection of the particle in the transition problem. However, for specific target states, the target site measurement approach can be extremely fast, as the motion is essentially ballistic [17].

While in this section, and this paper in general, we focused on comparisons to the results found for the detection protocol considered in [19–21], we would be remiss in not mentioning other works in the field of quantum random walks that make use of other measurement protocols and the broader effects of measurements on quantum-mechanical systems, such as [15,17,41–47].

X. SUMMARY

In this paper, we developed a theoretical framework for the study of quantum walks with repeated measurements of the position operator, which we have termed the measurement-induced quantum walk. In particular, we have focused on studying the first detection problem within this framework.

As shown in [1–6], both decoherence and measurements may induce classical features in a quantum walk. Our research both verifies and expands upon this known result, as we have shown that upon closer inspection of these classical features, nontrivial quantum effects can still be found. In the case of the infinite line, these effects can be seen using a large deviation theory and Edgeworth expansion. Additional nonclassical effects can be seen in this system by analyzing the Zeno limit using Kurtosis. Furthermore, while decoherence processes are important in the context of measurements and the transition between quantum and classical worlds, they are not sufficient to define a measured path of the particle. Thus monitoring is essential in the basic definition of quantum functionals such as the first hitting time, which we have studied in depth in our work. It will be interesting to study our model in the presence of decoherence.

One remarkable feature that we found of the return problem in a finite graph is that the mean $\langle n\rangle$ is quantized and equal to the size of the graph. This breaks down at exceptional sampling rates when the effective size of the system is smaller than the actual size, due to ergodicity breaking (see Fig. 13). Importantly, it remains an integer, and so does $\langle n\rangle$. For the transition problem, we have a very different behavior as $\langle n\rangle$ is certainly not an integer. Instead, it typically diverges close to exceptional sampling rates, but not always, as can be seen in Fig. 11. Although the discontinuities in $\langle n\rangle$ (such as those seen in Fig. 9) are very difficult to measure directly as any slight change in the sampling rate or noise from the environment will ruin this exceptional sampling rate, we can still observe the effect of these sampling rates in the divergence of the variance as is seen in Figs. 9 and 12. Hence to study the effects of exceptional sampling rates, one does not need to tune the system very precisely, and one may instead simply focus on the fluctuations. Furthermore, we have shown that in finite systems the convergence to the functionals of the walk, such as the survival probability or the mean number of detection attempts, slows down drastically close to exceptional sampling rates for both the return and transition problem.

For a particle on a one-dimensional infinite lattice, we found that F_n decays like $n^{-3/2}$. This is different from what was found in [19] for the same Hamiltonian when measuring only at the origin where the decay rate was found to be $F_n \sim n^{-3}$ with superimposed quantum oscillation. Hence the value of the exponent of the first detection probabilities depends on the observable used to define the problem. In our case, the exponent $3/2$ is the same as the one obtained for a regular classical random walk. Of course, this does not imply that the problem itself is classical, only that the exponent $3/2$ is. This finding is augmented by the fact that the rate at which the first detection probabilities converge to this asymptotic limit is highly dependent on the sampling rate, as very fast or very slow sampling delay the convergence, while for intermediate sampling rates the probabilities converge almost instantly.

In examining the shape of the probability vector on this lattice, we found that, outside of the Zeno limit, it takes the form of a Gaussian distribution, as expected. However, a closer examination using an Edgeworth expansion near the origin and a large-deviation theory near the tails of the distribution

revealed noteworthy corrections to this classical behavior. For example, the large deviation theory reveals the ballistic scaling, which is the hallmark of quantum walks in the absence of measurements, while the central part of the packet is Gaussian and hence diffusive in the classical sense.

ACKNOWLEDGMENTS

The support of the Israel Science Foundation's Grant No. 1898/17 is acknowledged. We thank David Kessler, Felix Thiel, Ruoyu Yin, and Quancheng Liu for discussions and comments.

APPENDIX A: DERIVATION OF F_n

In this Appendix, we present all of the steps leading to the derivation of Eq. (9) in detail.

1. The time evolution operator

We will start by showing that using G as the time evolution operator of the probability vector does in fact cause it to behave as we have described in Sec. III. We will prove $G\,|\rho(\tau n^+)\rangle = |\rho[\tau(n+1)^-]\rangle$ by induction.

For $n=0$ we get $G\,|\rho(0)\rangle = \sum_x |\,\langle x|e^{-i\tau H}|\psi_{\rm in}\rangle\,|^2\,|x\rangle$, which is simply the probability that the wave function collapsed to each of those sites. For $0<n$, we have $|\rho(\tau n)\rangle = \sum_x P_x^{\tau n}\,|x\rangle$, where by the induction hypotheses $P_x^{\tau n}$ is the probability that the wave function is localized to $|x\rangle$ at $t=\tau n$. The probability that $|\psi\rangle$ is localized to some arbitrary site $|y\rangle$ at $t=\tau(n+1)$ is $\sum_x P_x^{\tau n}P_{x\to y}$, where $P_{x\to y}$ is the probability that a wave function starting at $|x\rangle$ collapses to $|y\rangle$ after being operated on by $e^{-i\tau H}$, which is given by $|\,\langle y|e^{-i\tau h}|x\rangle\,|^2$. Operating on $|\rho(\tau n)\rangle$ with G, we get

$$G|\rho(\tau n)\rangle = \sum_x\left[\sum_{x'} P_{x'}^{\tau n}P_{x'\to x}\right]|x\rangle = \sum_x P_x^{\tau(n+1)}|x\rangle. \quad \text{(A1)}$$

$\sum_x P_x^{\tau(n+1)}\,|x\rangle$ equals $|\rho[\tau(n+1)]\rangle$ by the definition of P_n^t, so the proof is complete.

2. Evolution of the probability vector

In this subsection, we will derive Eq. (8). Note that in this subsection we use P_n to refer to the conditional probability that the wave function is localized to $|\psi_{\rm tar}\rangle$ at τn after having not been detected at $\psi_{\rm tar}$ in the past $n-1$ attempts, as opposed to F_n, which is the probability of first detecting the particle at $\psi_{\rm tar}$ on the nth measurement. The relation between the two is $F_n = P_n\Pi_{j=1}^{n-1}(1-P_j)$. We will also be making frequent use of the operator $D = |\psi_{\rm tar}\rangle\,\langle\psi_{\rm tar}|$.

For $n=1$, Eq. (8) follows directly from the defining property of G, which was proven in the previous subsection of this Appendix, and the probability that the wave function is localized to $\psi_{\rm tar}$ is $F_1 = P_1 = \langle\psi_{\rm tar}|G|\psi_{\rm in}\rangle$. If the system was not measured to be in the state $\psi_{\rm tar}$, then at $t=\tau+\epsilon$ ($\epsilon\in\mathbb{R}^+, \epsilon\to 0^+$) the probability vector is $|\rho(\tau+\epsilon)\rangle = N(1-D)\,|\rho(\tau)\rangle$, where N is the normalization of the probability, which in this case is $N=(1-P_1)^{-1}$. Continuing to evolve the vector in time, we find that $|\rho(2\tau)\rangle = \frac{G(1-D)G|\psi_{\rm in}\rangle}{1-P_1}$. If the system was not found at $\psi_{\rm tar}$ again, then the probability vector is $|\rho(2\tau+\epsilon)\rangle = \frac{(1-D)G(1-D)G|\psi_{\rm in}\rangle}{(1-P_1)(1-P_2)}$.

This iteration procedure is repeated, with the operator $G(1-D)$ removing the component that was not detected at the target site and evolving the probability vector in time and the normalization $(1-P_j)^{-1}$ being added with each such failed detection attempt. After continuing in this manner for τn time, we have

$$|\rho(\tau n)\rangle = \frac{[G(1-D)]^{n-1}G\,|\psi_{\rm in}\rangle}{\Pi_{j=1}^{n-1}(1-P_j)}. \quad \text{(A2)}$$

Applying $\langle\psi_{\rm tar}|$ to both sides and multiplying by $\Pi_{j=1}^{n-1}(1-P_j)$, we have

$$P_n\Pi_{j=1}^{n-1}(1-P_j) = \langle\psi_{\rm tar}|[G(1-D)]^{n-1}G|\psi_{\rm in}\rangle\,. \quad \text{(A3)}$$

The left-hand side of this equation is the probability that the nth measurement attempt succeeded and all previous attempts failed, which is how we defined F_n. Hence, the derivation of Eq. (8) is complete.

3. Renewal equation derivation

In this section, we will show by induction that

$$[G(\mathbb{1}-D)]^{n-1}G|\psi_{\rm in}\rangle = G^n|\psi_{\rm in}\rangle - \sum_{j=1}^{n-1}F_jG^{n-j}|\psi_{\rm tar}\rangle. \quad \text{(A4)}$$

For $n=1$, it is easy to see that both are just $G\,|\psi_{\rm in}\rangle$. We will now assume that the equation is correct for n, and we prove that it follows for $n+1$.

Operating on the left-hand side of Eq. (A4) with $G(\mathbb{1}-D)$, we get $[G(\mathbb{1}-D)]^nG\,|\psi_{\rm in}\rangle$. Operating on the right-hand side with $G(\mathbb{1}-D)$, we get

$$G^{n+1}|\psi_{\rm in}\rangle - \sum_{j=1}^{n-1}F_jG^{n+1-j}|\psi_{\rm tar}\rangle - \left[\langle\psi_{\rm tar}|G^n|\psi_{\rm in}\rangle - \sum_{j=1}^{n-1}F_j\langle\psi_{\rm tar}|G^{n-j}|\psi_{\rm tar}\rangle\right]G|\psi_{\rm tar}\rangle. \quad \text{(A5)}$$

Notice that the segment in square brackets in Eq. (A5) is F_n. After applying this change and making the rightmost expression part of the sum, we get

$$[G(\mathbb{1}-D)]^nG|\psi_{\rm in}\rangle = G^{n+1}|\psi_{\rm in}\rangle - \sum_{j=1}^{n}F_jG^{n+1-j}|\psi_{\rm tar}\rangle. \quad \text{(A6)}$$

This equation is the same as (A4) but for $n+1$. Hence, the proof is complete. To get the equivalence of Eqs. (8) and (9) from this, simply operate on Eq. (A6) with $\langle\psi_{\rm tar}|$.

APPENDIX B: EIGENVALUES AND EIGENSTATES OF G

To complete the derivations of the general formulas for the moments of the generating function, some general properties of G's eigenvalues and eigenstates are necessary.

1. All eigenvalues of G are $\leqslant 1$

According to the Gershgorin circle theorem [48], all of G's eigenvalues lie within "Gershgorin disks" $D(G_{ii}, R_i)$, which

are disks in the complex plane where G_{ii} is the center of the disk and $R_i = \sum_{i\neq j} |G_{ij}|$ is the radius of the disk. Since G is Hermitian, we can replace the statement of the theorem with $\forall_\lambda \exists_i : |G_{ii} - \lambda| \leqslant R_i$, where λ are the eigenvalues of G. Since the total probability of a particle to jump to some other site from any initial site is 1, we can replace R_i with $1 - G_{ii}$ and use that to rewrite the previous equation as follows: $\forall_\lambda \exists_i : |G_{ii} - \lambda| \leqslant 1 - G_{ii}$. If $G_{ii} \leqslant \lambda$, it easily follows that $\forall |\lambda| \leqslant 1$. Otherwise, if $\lambda < G_{ii}$, then it is also less than or equal to 1 since $\forall_i G_{ii} \leqslant 1$.

2. The vector $|\phi\rangle = \frac{1}{\sqrt{|X|}} \sum_x |x\rangle$ is an eigenstate of G

$$G\,|\phi\rangle = \frac{1}{\sqrt{|X|}} \sum_x \left[\sum_{x'} |\,\langle x|e^{-iH\tau}|x'\rangle\,|^2 \right] |x\rangle = |\phi\rangle\,. \quad \text{(B1)}$$

The term in the square brackets is the total probability of the particle to be detected anywhere after the detection attempt, which is just 1 from the normalization of the wave function.

APPENDIX C: NONLOCAL INITIAL CONDITIONS

Throughout the paper, we have assumed that $|\psi_{\text{in}}\rangle$ is a localized state for the sake of simplicity, however it should be noted that our method also works for nonlocal initial wave functions after some slight modifications which will be detailed in this Appendix. The first and most important of these modifications is that rather than simply setting $|\rho(0)\rangle = |\psi_{\text{in}}\rangle$, we will first need to localize the wave function using the measurement at time τ. This step is needed since the stochastic matrix G can only be used to evolve the system in time if the wave function is localized,

$$|\rho(\tau)\rangle = \sum_{x\in X} |\,\langle x|e^{-iH\tau}|\psi_{\text{in}}\rangle\,|^2\,|x\rangle\,. \quad \text{(C1)}$$

After finding the probability vector at time τ, we will subtract the first detection probability $F_1 = \langle\psi_{\text{tar}}|\rho(\tau)\rangle$ from it,

$$|\rho(\tau^+)\rangle = \sum_{x\in X/\{\psi_{\text{tar}}\}} |\,\langle x|e^{-iH\tau}|\psi_{\text{in}}\rangle\,|^2\,|x\rangle\,. \quad \text{(C2)}$$

Once this process is done, the wave function is localized to some site x_1 and we can simply continue to evolve this probability vector in time using G as if it were the initial state of our system. However, it should be noted that if we simply calculate the generating function from this probability vector as it is, the indices of the probabilities will be shifted,

$$\widetilde{F(z)}' = \sum_{n=1}^{\infty} F_{n+1} z^n = \frac{\langle\psi_{\text{tar}}|\widetilde{G(z)}|\rho(\tau^+)\rangle}{1 + \langle\psi_{\text{tar}}|\widetilde{G(z)}|\psi_{\text{tar}}\rangle}. \quad \text{(C3)}$$

We can compensate for this by multiplying the generating function by z and adding zF_1 to it,

$$\widetilde{F(z)} = zF_1 + z\widetilde{F(z)}'. \quad \text{(C4)}$$

Once this step is done, we can use the generating function in just the same manner as we would in the case where $|\psi_{\text{in}}\rangle$ is localized. However, it should also be noted that the general results we have derived in Sec. V no longer apply.

APPENDIX D: DISCONTINUOUS JUMPS OF $\langle n\rangle$ IN THE TRANSITION PROBLEM

In this Appendix, we derive a general formula for the value of $\langle n\rangle$ at an exceptional sampling rate when it does not diverge, and we demonstrate that when not diverging, it often jumps discontinuously. We will start by examining the behavior of the function $g(z)$ defined in Eq. (27) in the limit where $z \to 1$ and $\tau \to \tau_{\text{ex}}$, where τ_{ex} is an exceptional sampling rate of the system. As a reminder, the function $g(z)$ is

$$g(z) = \sum_\lambda \sum_{k=1}^{g_\lambda} \sum_{j=1}^{g_1} \frac{\lambda z}{1-\lambda z} f(|\lambda_k\rangle\,,|1_j\rangle),$$

$$f(|\lambda_k\rangle\,,|1_j\rangle) = \langle\psi_{\text{tar}}|1_j\rangle\,\langle 1_j|\psi_{\text{in}}\rangle\,|\,\langle\psi_{\text{tar}}|\lambda_k\rangle\,|^2 - \langle\psi_{\text{tar}}|\lambda_k\rangle\,\langle\lambda_k|\psi_{\text{in}}\rangle\,|\,\langle\psi_{\text{tar}}|1_j\rangle\,|^2. \quad \text{(D1)}$$

The problematic terms in the sum over λ_k are the terms whose eigenvalue is 1. If the inner sum over j is nonzero for any of them, then $\langle n\rangle$ will diverge. Assuming that it is zero and then simplifying, we get the following equation for the value of $\langle n\rangle$ at an exceptional point that does not cause it to diverge:

$$\langle n\rangle_{\text{ex}} = A^{-1} + A^{-2} \sum_{\lambda\neq 1} \sum_{k=1}^{g_\lambda} \sum_{j=1}^{g_1} \frac{\lambda}{1-\lambda} f(|\lambda_k\rangle\,,|1_j\rangle), \quad \text{(D2)}$$

where $A = \sum_{k=1}^{g_1} |\,\langle\psi_{\text{tar}}|1_k\rangle\,|^2$. Although the assumption that the inner sum is zero may seem unlikely, it is satisfied fairly often. We show an example of this in Fig. 11, and this discontinuous jump is fairly common in other systems as well.

One additional assumption we need to make is that for at least one of the eigenstates whose eigenvalue is 1 besides $|\phi\rangle$, its projection onto the target state is nonzero: $\langle\psi_{\text{tar}}|\lambda_k\rangle \neq 0$. Without this assumption, we will get $\langle n\rangle_{\text{ex}} = \langle n\rangle$. We think that this assumption is justified by the fact that the projection of the target site onto the eigenstates of G appears in both the denominator and numerator of the generating function, so if the projections of all of these eigenstates are zero, this means that this set of eigenstates did not influence the statistics of the first detection time to begin with. It is fairly simple to invent a Hamiltonian describing a graph where some parts of the graph cannot be reached from others. For any such Hamiltonian, it is clear that the eigenstates describing one part of the system will not affect the behavior of a walk on a different part that cannot be reached, meaning that all the projections would be zero. In such cases, our assumption is wrong and the exceptional sampling rate in question will not affect the statistics of the measurement-induced quantum walk. Keep in mind that all that was shown in this section does not mean that $\langle n\rangle$ necessarily discontinuously jumps if it does not diverge, as the two expressions can still equal each other. However, given the assumption that the projection onto the set of exceptional eigenstates is nonzero, there is also no particular reason why the two expressions for $\langle n\rangle$ should equal each other, so more often than not they will be different, as can be seen in Fig. 11.

APPENDIX E: TWO-LEVEL SYSTEM

In this Appendix, we solve the first detection problem for a two-level system in detail to present the steps one would need

to perform to use our formalism in practice. The Hamiltonian of the two-level system is given by

$$H = -\gamma(|0\rangle\langle 1| + |1\rangle\langle 0|) + U|1\rangle\langle 1|. \tag{E1}$$

As previously mentioned in Sec. II, this Hamiltonian can describe a particle hopping between two distinct sites or any arbitrary two-state quantum system where one state has higher energy than the other, such as a spin-1/2 particle in a magnetic field where the measurement is of the orientation of the spin ($X = \{|L\rangle, |R\rangle\}$), for example. Note that our method is only applicable to this example if the axis of measurement is not parallel to the orientation of the magnetic field, since in that case the states being measured are the eigenstates of the Hamiltonian, which would cause G to simply be the identity matrix.

The first step to finding either the return or transition probabilities is to diagonalize G. To do this, we first diagonalize the Hamiltonian to obtain the time evolution of every initial condition ($|0\rangle$ and $|1\rangle$) and then we use those results in Eq. (6) to compute G:

$$G = \begin{pmatrix} \frac{U^2+2\gamma^2[1+\cos(\tau\sqrt{U^2+4\gamma^2})]}{U^2+4\gamma^2} & \frac{2\gamma^2[1-\cos(\tau\sqrt{U^2+4\gamma^2})]}{U^2+4\gamma^2} \\ \frac{2\gamma^2[1-\cos(\tau\sqrt{U^2+4\gamma^2})]}{U^2+4\gamma^2} & \frac{U^2+2\gamma^2[1+\cos(\tau\sqrt{U^2+4\gamma^2})]}{U^2+4\gamma^2} \end{pmatrix}. \tag{E2}$$

After this step is done, we diagonalize G to find its eigenstates and eigenvalues,

$$|\lambda_1\rangle = \frac{1}{\sqrt{2}}(|0\rangle + |1\rangle) = |\phi\rangle, \quad |\lambda_2\rangle = \frac{1}{\sqrt{2}}(-|0\rangle + |1\rangle),$$

$$\lambda_1 = 1, \quad \lambda_2 = \frac{U^2 + 4\gamma^2\cos(\tau\sqrt{U^2+4\gamma^2})}{U^2+4\gamma^2}. \tag{E3}$$

Notice that $|\lambda_2| \leqslant 1$, as expected. Exceptional sampling rates are found when the cosine found in λ_2 equals 1, which causes the eigenvalue itself to equal 1.

Using these we can now easily calculate the first detection generating function Eq. (11) for any transition on the system in the $|0\rangle, |1\rangle$ basis using Eq. (13). Note that since the on-site energy U only appears squared, both possible transition problems on this graph behave identically, the same for the two possible return problems. Using Eq. (E3) and the aforementioned remark that the cosine should equal 1, we have

$$\frac{4\pi^2k^2}{\tau^2} = U^2 + 4\gamma^2, \tag{E4}$$

where k is a nonzero natural number (assuming $\gamma \neq 0$). Choosing values of τ, γ, and U, which satisfy Eq. (E4), causes the transition matrix G to become the identity matrix. From this, it is easy to see that for exceptional sampling rates, the particle will be detected at the first attempt with certainty. For nonexceptional sampling rates, we can use the general results derived in Sec. V, which tell us that in the return problem, $P_{\text{det}} = 1$ and $\langle n\rangle = 2$. These results can also be confirmed by evaluating the generating function and its derivative directly. We can obtain the variance using either Eq. (26) or by taking the second derivative of $\widetilde{F}(z)$. Either way, we will find that it goes like $\Delta n^2 \sim (1-\lambda_2)^{-1}$. Note that although the variance goes to infinity as λ_2 goes to 1, when λ_2 is 1 the variance becomes zero. This is because at those sampling rates the particle is detected at the first attempt with probability 1.

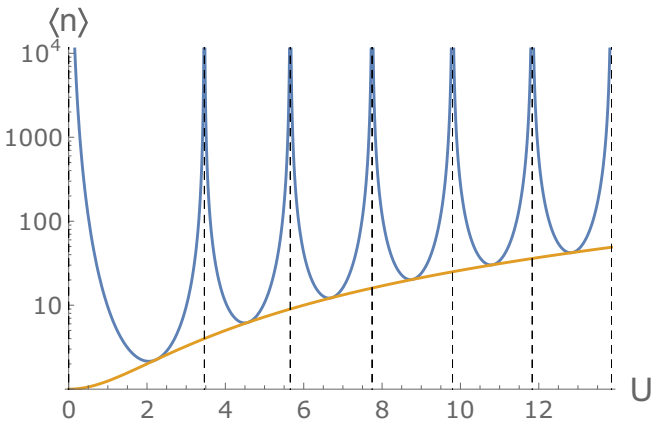

FIG. 18. The average number of measurements until first detection in the transition from $|\psi_{\text{in}}\rangle = |0\rangle$ to $|\psi_{\text{tar}}\rangle = |1\rangle$ for the two-level system model whose Hamiltonian is given in Eq. (E1) as a function of the on-site energy U plotted in blue, where we set $\tau = \pi$ and $\gamma = 1$. The average diverges at every exceptional value of U while also tending to increase overall like $U^2/4$ (plotted in orange). The exceptional energy differences are denoted by the dashed vertical lines. The variance (not plotted) behaves very similarly.

Next, we will briefly examine the transition from $|0\rangle$ to $|1\rangle$. Keep in mind that since $|\langle 0|e^{-i\tau H}|1\rangle|^2 = |\langle 1|e^{-i\tau H}|0\rangle|^2$, the behavior of this transition is identical to the one from $|1\rangle$ to $|0\rangle$, and the choice to examine one and not the other is arbitrary. As expected based on Sec. V, we find that P_{det} is 1 for all nonexceptional combinations of U, γ, and τ, and that for the exceptional ones the particles are never detected. In addition, we find that the average and variance both diverge near these values, although at the values themselves they jump to zero since all probabilities become zero. We plot the average as a function of the on-site energy in Fig. 18.

APPENDIX F: INFINITE LINE RETURN PROBLEM PROBABILITY VECTOR DERIVATION

In this Appendix, we derive the Fourier transform of the probability vector for the return problem on the infinite line lattice whose Hamiltonian is given by Eq. (38) and whose initial condition is $|\psi_{\text{in}}\rangle = |0\rangle$. We start with the general form of the probability vector at time $t = \tau n$, which, for the time evolution operator given in Eq. (40), is given by

$$|\rho(\tau n)\rangle = \left(\sum_{x,x'=-\infty}^{\infty} |J_{x-x'}(2\gamma\tau)|^2 |x\rangle\langle x'|\right)^n |0\rangle. \tag{F1}$$

Notice that the expression we have arrived at is the discrete convolution of $|J_x(2\gamma\tau)|^2$ with itself n times with respect to x. Using the discrete convolution theorem, its Fourier transform equals the nth power of the Fourier transform of $|J_x(2\gamma\tau)|^2$. To find the Fourier transform of $|J_x(2\gamma\tau)|^2$, we will start with the generating function of the Bessel functions:

$$e^{\frac{z}{2}(t-\frac{1}{t})} = \sum_{x=-\infty}^{\infty} t^x J_x(z). \tag{F2}$$

Setting $t = e^{i\theta}$ and integrating from zero to 2π, we get

$$\frac{1}{2\pi}\int_0^{2\pi} e^{iz\sin(\theta)}d\theta = J_0(z). \tag{F3}$$

Next, we make two copies of the generating function. In one copy, we set $t = e^{i\theta}$, and in the other copy we take the complex conjugate and set $t = e^{i(\theta+k)}$. We then multiply these two by each other to obtain

$$e^{iz[\sin(\theta)-\sin(\theta+k)]} = \sum_{x,y=-\infty}^{\infty} e^{-iky}e^{i\theta(x-y)}J_x(z)[J_y(z)]^*. \tag{F4}$$

Dividing by 2π and integrating from zero to 2π with respect to θ, we get

$$\frac{1}{2\pi}\int_0^{2\pi} e^{iz[\sin(\theta)-\sin(\theta+k)]}d\theta = \sum_{y=-\infty}^{\infty} e^{-iky}|J_y(z)|^2. \tag{F5}$$

To evaluate the integral on the left-hand side, we make use of the fact that we can write $\sin(\theta) - \sin(\theta + k)$ as $a\sin(\theta + b)$, where $a = 2\sin(k/2)$, and we do not need to find b since the integral is over the whole cycle anyway,

$$\frac{1}{2\pi}\int_0^{2\pi} e^{2iz\sin(k/2)\sin(\theta+b)}d\theta = \sum_{y=-\infty}^{\infty} e^{-iky}|J_y(z)|^2. \tag{F6}$$

Using Eqs. (F3) and (F6), we find that the Fourier transform is

$$\sum_{y=-\infty}^{\infty} e^{-iky}|J_y(2\gamma\tau)|^2 = J_0\left(4\gamma\tau\sin\left(\frac{k}{2}\right)\right). \tag{F7}$$

Raising this expression to the nth power, we find that the Fourier transform of the probability vector at time $t = \tau n$ is

$$\sum_k e^{-ikx}\langle x|\rho(\tau n)\rangle = J_0\left(4\gamma\tau\sin\left(\frac{k}{2}\right)\right)^n. \tag{F8}$$

Taking the inverse Fourier transform, this shows that the probability vector is given by

$$\langle x|\rho(\tau n)\rangle = \frac{1}{2\pi}\int_0^{2\pi} e^{ikx}J_0\left(4\gamma\tau\sin\left(\frac{k}{2}\right)\right)^n. \tag{F9}$$

APPENDIX G: SADDLE POINT APPROXIMATIONS DERIVATION

In this Appendix, we derive the results presented in Sec. VIII B. These solutions are based on the methods presented in [39], and they can be briefly summarized in that we can obtain an approximate expression for the probability vector using

$$P_{x,n} \approx \frac{1}{\sqrt{2\pi K''(\hat{u})}}\exp\left(K(\hat{u}) - \hat{u}x\right),$$
$$K(u) = \ln\langle\exp(ux)\rangle = n\ln\left(I_0(4\gamma\tau\sinh(u/2))\right), \tag{G1}$$

where $\hat{u}$ satisfies $K'(\hat{u}) = x$. In our case, it is the solution to the equation

$$x = 2n\gamma\tau\frac{I_1(4\gamma\tau\sinh(\hat{u}/2))}{I_0(4\gamma\tau\sinh(\hat{u}/2))}\cosh(\hat{u}/2). \tag{G2}$$

Looking at the region where $x \sim n$ by setting $x = 2n\gamma\tau l$, we have the equation

$$l = \frac{I_1(4\gamma\tau\sinh(\hat{u}/2))}{I_0(4\gamma\tau\sinh(\hat{u}/2))}\cosh(\hat{u}/2). \tag{G3}$$

We will solve this equation for different regions of the probability vector by using different appropriate approximations. Where neither approximation applies, we solve Eq. (G2) numerically.

1. Small l solution

This solution corresponds to the center of the distribution, where from both the central limit theorem and the previously presented Edgeworth series solution we expect to find a Gaussian distribution. For a small l we can approximate the right-hand side of Eq. (G3) using a first-order Taylor series, which gives us

$$l = \gamma\tau\hat{u}, \quad \hat{u} = \frac{x}{2n\gamma^2\tau^2} = \frac{x}{\Delta x^2}. \tag{G4}$$

As a reminder, x and Δx^2 are unitless. Plugging this result into Eq. (G1) and adding one additional minor approximation, we obtain a Gaussian distribution as expected:

$$P_{x,n} = \frac{1}{\sqrt{2\pi\,\Delta x^2}}\exp\left(-\frac{x^2}{2\Delta x^2}\right),$$
$$P_{x,n} = \frac{1}{\sqrt{4\pi n\gamma^2\tau^2}}\exp\left(-\frac{x^2}{4n\gamma^2\tau^2}\right). \tag{G5}$$

2. Large l solution

This solution corresponds to the far tails of the distribution, and we expect it to display very strong decay to zero. For this region, the right-hand side of Eq. (G3) converges to just the hyperbolic cosine, and we get

$$l = \cosh(\hat{u}/2), \quad \hat{u} = 2\,\mathrm{arccosh}(l). \tag{G6}$$

Plugging these into Eq. (G1), we make use of the following additional approximations:

$$\frac{I_1(4\gamma\tau l)}{I_0(4\gamma\tau l)} \approx \frac{I_2(4\gamma\tau l)}{I_0(4\gamma\tau l)} \approx 1. \tag{G7}$$

This gives us the following approximation for the probability vector:

$$P_{x,n} = \frac{1}{2\pi n\gamma\tau\sqrt{\left(\frac{x}{2\gamma\tau n}\right)^2 - 1}}\frac{I_0\left(4\gamma\tau\sqrt{\left(\frac{x}{2\gamma\tau n}\right)^2 - 1}\right)^n}{\exp\left[2x\,\mathrm{arccosh}\left(\frac{x}{2\gamma\tau n}\right)\right]}. \tag{G8}$$

In the limit we took of $1 \ll l$, by extension we also have $1 \ll l \ll n \ll x$, meaning that the term in the denominator in Eq. (G8) is much greater than the one in the numerator, demonstrating the rapid decay to zero that we expected.

APPENDIX H: DERIVATION OF THE $\langle n\rangle$ AND Δn^2 EQUATIONS

In this Appendix, we show the derivation of Eqs. (24) and (26) in detail, as well as a more general formula for Δn^2 than what we presented in Sec. V. As a reminder, we are

starting with Eq. (22) in the $|\psi_{\rm in}\rangle = |\psi_{\rm tar}\rangle$ case, and our goal is to find the limit as $z \to 1$ of its first and second derivative with respect to z. For this section, we introduce some new notation to shorten the following equations. First, we abbreviate the sums over the eigenstates $\sum_\lambda \sum_{k=1}^{g_\lambda} |\lambda_k\rangle$ as just $\sum_\lambda |\lambda\rangle$. Each such sum is over all eigenstates unless stated otherwise, i.e., $\sum_{\lambda=1}$ is only over eigenstates whose eigenvalue is 1 and $\sum_{\lambda\neq 1}$ is over all other eigenvalues. Secondly, we abbreviate the squared projection of the initial state $|\psi_{\rm in}\rangle$ onto each eigenstate as $\psi_\lambda = |\langle\psi_{\rm in}|\lambda\rangle|^2$.

Starting with $\langle n\rangle$, we add and subtract 1 to the numerator in Eq. (22) and rewrite it using the shorthand notation we have introduced:

$$\widetilde{F(z)} = \frac{1+\sum_\lambda \psi_\lambda \frac{\lambda z}{1-\lambda z} - 1}{1+\sum_\lambda \psi_\lambda \frac{\lambda z}{1-\lambda z}} = 1 - \frac{1}{1+\sum_\lambda \psi_\lambda \frac{\lambda z}{1-\lambda z}}. \tag{H1}$$

Taking the first derivative, we get

$$\frac{d}{dz}\widetilde{F(z)} = \frac{\sum_\lambda \psi_\lambda \frac{\lambda}{(1-\lambda z)^2}}{\left(1+\sum_\lambda \psi_\lambda \frac{\lambda z}{1-\lambda z}\right)^2}. \tag{H2}$$

Next, we multiply and divide the generating function by $(1-z)^2$,

$$\frac{d}{dz}\widetilde{F(z)} = \frac{\sum_\lambda \psi_\lambda \lambda \frac{(1-z)^2}{(1-\lambda z)^2}}{\left(1-z+\sum_\lambda \psi_\lambda \lambda z \frac{1-z}{1-\lambda z}\right)^2}. \tag{H3}$$

Written like this, we can see that the reason exceptional eigenvalues are significant is that only the eigenstates whose eigenvalue is 1 will remain after we take the limit $z \to 1$. Taking the limit, we easily obtain Eq. (24),

$$\lim_{z\to 1}\frac{d}{dz}\widetilde{F(z)} = \frac{\sum_{\lambda=1}\psi_\lambda}{\left(\sum_{\lambda=1}\psi_\lambda\right)^2} = \frac{1}{\sum_{\lambda=1}\psi_\lambda}. \tag{H4}$$

For the variance, we start by first relating it to $\langle n\rangle$ and the second derivative of the generating function,

$$\begin{aligned}\Delta n^2 &= \langle n^2\rangle - \langle n\rangle^2 \\ &= \frac{d}{dz}\left(z\frac{d}{dz}\right)\widetilde{F(z)}|_{z\to 1} - \langle n\rangle^2 \\ &= \frac{d^2}{dz^2}\widetilde{F(z)}|_{z\to 1} + \langle n\rangle - \langle n\rangle^2 .\end{aligned} \tag{H5}$$

Next, we need to find the value of the second derivative at $z \to 1$. Taking the derivative of Eq. (H2), we get

$$\frac{d^2}{dz^2}\widetilde{F(z)} = \left[\sum_\lambda \psi_\lambda \frac{2\lambda^2}{(1-\lambda z)^3} + \sum_{\lambda,\Lambda}\psi_\lambda\psi_\Lambda \frac{2\lambda^2}{(1-\lambda z)^3}\frac{\Lambda z}{1-\Lambda z} - 2\sum_{\lambda,\Lambda}\psi_\lambda\psi_\Lambda \frac{\lambda}{(1-\lambda z)^2}\frac{\Lambda}{(1-\Lambda z)^2}\right]\left(1+\sum_\lambda \psi_\lambda \frac{\lambda z}{1-\lambda z}\right)^{-3}. \tag{H6}$$

Since the limit of a sum is the sum of the limits if both limits exist, we can simplify our equation slightly by first finding the limit of the first sum which appears in the numerator and later find the limit of the rest of the sums. We can compute this first limit easily in the same way we did for Eq. (H4) by multiplying and dividing by $(1-z)^3$ so that after taking the limit, only the eigenstates whose eigenvalue is 1 will remain,

$$\lim_{z\to 1}\frac{\sum_\lambda \psi_\lambda \frac{2\lambda^2}{(1-\lambda z)^3}}{\left(1+\sum_\lambda \psi_\lambda \frac{\lambda z}{1-\lambda z}\right)^3} = \lim_{z\to 1}\frac{\sum_\lambda \psi_\lambda 2\lambda^2 \frac{(1-z)^3}{(1-\lambda z)^3}}{\left(1-z+\sum_\lambda \psi_\lambda \lambda z \frac{1-z}{1-\lambda z}\right)^3} = \frac{2}{\left(\sum_{\lambda=1}\psi_\lambda\right)^2} = 2\langle n\rangle^2 . \tag{H7}$$

Next, to find the limit of the two double sums, we will first combine them into a single double sum. As we do this, we also multiply the whole expression by the $(1-z)^3$ which originates in the denominator of Eq. (H6),

$$\begin{aligned}&(1-z)^3\left[\sum_{\lambda,\Lambda}\psi_\lambda\psi_\Lambda \frac{2\lambda^2}{(1-\lambda z)^3}\frac{\Lambda z}{1-\Lambda z} - 2\sum_{\lambda,\Lambda}\psi_\lambda\psi_\Lambda \frac{\lambda}{(1-\lambda z)^2}\frac{\Lambda}{(1-\Lambda z)^2}\right] \\ &= \sum_{\lambda,\Lambda}\psi_\lambda\psi_\Lambda \frac{\lambda\Lambda}{(1-\lambda z)^3}\frac{(1-z)^3}{(1-\Lambda z)^2}[2\lambda z(1-\Lambda z) - 2(1-\lambda z)] \\ &= \sum_{\lambda,\Lambda}\psi_\lambda\psi_\Lambda \frac{\lambda\Lambda}{(1-\lambda z)^3}\frac{(1-z)^3}{(1-\Lambda z)^2}(4\lambda z - 2\lambda\Lambda z^2 - 2).\end{aligned} \tag{H8}$$

To see what elements of this double sum reduce to zero in the limit and which will remain, we will break it apart into four sums depending on whether the eigenvalues of the eigenstates being summed over equal 1 or not,

$$\begin{aligned}&\sum_{\substack{\lambda=1\\ \Lambda=1}}\psi_\lambda\psi_\Lambda \frac{1}{(1-z)^3}\frac{(1-z)^3}{(1-z)^2}(4z-2z^2-2) + \sum_{\substack{\lambda=1\\ \Lambda\neq 1}}\psi_\lambda\psi_\Lambda \frac{\Lambda}{(1-z)^3}\frac{(1-z)^3}{(1-\Lambda z)^2}(4z-2\Lambda z^2-2) \\ &+ \sum_{\substack{\lambda\neq 1\\ \Lambda=1}}\psi_\lambda\psi_\Lambda \frac{\lambda}{(1-\lambda z)^3}\frac{(1-z)^3}{(1-z)^2}(4\lambda z-2\lambda z^2-2) + \sum_{\substack{\lambda\neq 1\\ \Lambda\neq 1}}\psi_\lambda\psi_\Lambda \frac{\lambda\Lambda}{(1-\lambda z)^3}\frac{(1-z)^3}{(1-\Lambda z)^2}(4\lambda z-2\lambda\Lambda z^2-2).\end{aligned} \tag{H9}$$

We can see here that in the limit only the first two sums will remain whereas the other two will go to zero. After taking the limit and simplifying, we get

$$-2\sum_{\substack{\lambda=1\\ \Lambda=1}}\psi_\lambda\psi_\Lambda + 2\sum_{\substack{\lambda=1\\ \Lambda\neq 1}}\psi_\lambda\psi_\Lambda\frac{\Lambda}{1-\Lambda}. \tag{H10}$$

Putting this result together with Eq. (H7) in Eq. (H5), we obtain a general formula for the variance which is correct for all sampling rates,

$$\Delta n^2 = \langle n\rangle + \langle n\rangle^2 + \langle n\rangle^3\left(-2\sum_{\substack{\lambda=1\\ \Lambda=1}}\psi_\lambda\psi_\Lambda + 2\sum_{\substack{\lambda=1\\ \Lambda\neq 1}}\psi_\lambda\psi_\Lambda\frac{\Lambda}{1-\Lambda}\right). \tag{H11}$$

For nonexceptional sampling rates, the only term in the sum over eigenstates whose eigenvalue is 1 is the $|\phi\rangle$ term, which is just $|X|^{-1}$, and the expression can be simplified to Eq. (26).

[1] V. Kendon, Math. Structures Comput. Sci. **17**, 1169 (2007).
[2] A. Romanelli, R. Siri, G. Abal, A. Auyuanet, and R. Donangelo, Physica A **347**, 137 (2005).
[3] T. A. Brun, H. A. Carteret, and A. Ambainis, Phys. Rev. A **67**, 032304 (2003).
[4] T. A. Brun, H. A. Carteret, and A. Ambainis, Phys. Rev. Lett. **91**, 130602 (2003).
[5] C. Liu and N. Petulante, Phys. Rev. E **81**, 031113 (2010).
[6] R. Srikanth, S. Banerjee, and C. M. Chandrashekar, Phys. Rev. A **81**, 062123 (2010).
[7] S. N. Majumdar, Curr. Sci. **89**, 2076 (2005).
[8] S. Redner, *A Guide to First-Passage Processes* (Cambridge University Press, Cambridge, 2001), pp. 17–21.
[9] B. D. Hughes, *Random Walks and Random Environments* (Clarendon, Oxford, 1995).
[10] O. Bénichou and R. Voituriez, Phys. Rep. **539**, 225 (2014).
[11] A. J. Bray, S. N. Majumdar, and G. Schehr, Adv. Phys. **62**, 225 (2013).
[12] R. Metzler, G. Oshanin, and S. Redner, *First-Passage Phenomena and Their Applications* (World Scientific, Singapore, 2014).
[13] M. Kac, Trans. Am. Math. Soc. **65**, 1 (1949).
[14] F. A. Grunbaum, L. Velázquez, A. H. Werner, and R. F. Werner, Commun. Math. Phys. **320**, 543 (2012).
[15] S. Dhar, S. Dasgupta, A. Dhar, and D. Sen, Phys. Rev. A **91**, 062115 (2015).
[16] S. Dhar, S. Dasgupta, and A. Dhar, J. Phys. A **48**, 115304 (2015).
[17] H. Krovi and T. A. Brun, Phys. Rev. A **73**, 032341(R) (2006).
[18] H. Krovi and T. A. Brun, Phys. Rev. A **75**, 062332 (2007).
[19] H. Friedman, D. A. Kessler, and E. Barkai, Phys. Rev. E **95**, 032141 (2017).
[20] Q. Liu, R. Yin, K. Ziegler, and E. Barkai, Phys. Rev. Research **2**, 033113 (2020).
[21] R. Yin, K. Ziegler, F. Thiel, and E. Barkai, Phys. Rev. Research **1**, 033086 (2019).
[22] O. Mülken and A. Blumen, Phys. Rep.-Rev. Sect. Phys. Lett. **502**, 37 (2011).
[23] R. Metzler, G. Oshanin, and S. Redner, *First-Passage Phenomena and Their Applications* (World Scientific, Singapore, 2014).
[24] F. Thiel, E. Barkai, and D. A. Kessler, Phys. Rev. Lett. **120**, 040502 (2018).
[25] F. L. H. Brown, Acc. Chem. Res. **39**, 363 (2006).
[26] J. Yi, P. Talkner, and G.-L. Ingold, Phys. Rev. A **84**, 032121 (2011).
[27] F. Thiel, I. Mualem, D. A. Kessler, and E. Barkai, Phys. Rev. Research **2**, 023392 (2020).
[28] F. Thiel, I. Mualem, D. Meidan, E. Barkai, and D. A. Kessler, Phys. Rev. Research **2**, 043107 (2020).
[29] F. Thiel, I. Mualem, D. Kessler, and E. Barkai, Entropy **23**, 595 (2021).
[30] O. Bénichou, T. Guérin, and R. Voituriez, J. Phys. A **48**, 163001 (2015).
[31] E. W. Weisstein, Eigenvector. From MathWorld—A Wolfram Web Resource, last visited on 21/8/2021.
[32] D. Hartich and A. Godec, J. Stat. Mech. (2019) 024002.
[33] S. Fisk, arXiv:math/0502408 [math.CA], Amer. Math. Monthly **112**, 118 (2005).
[34] H. Zhao, J. Vovrosh, F. Mintert, and J. Knolle, Phys. Rev. Lett. **124**, 160604 (2020).
[35] Z. Papić, arXiv:2108.03460 [cond-mat.quant-gas].
[36] M. Abramowitz and I. Stegun, *Handbook of Mathematical Functions* (Dover, New York, 1972).
[37] F. Y. Edgeworth, J. R. Statist. Soc. **69**, 497 (1906).
[38] H. B. Perets, Y. Lahini, F. Pozzi, M. Sorel, R. Morandotti, and Y. Silberberg, Phys. Rev. Lett. **100**, 170506 (2008).
[39] H. E. Daniels, Ann. Math. Statist. **25**, 631 (1954).
[40] F. Thiel, D. A. Kessler, and E. Barkai, Phys. Rev. A **102**, 022210 (2020).
[41] M. Wampler, B. J. J. Khor, G. Refael, and I. Klich, arXiv:2108.05906 [quant-ph].
[42] J. Thingna and P. Talkner, Phys. Rev. A **102**, 012213 (2020).
[43] M. Varbanov, H. Krovi, and T. A. Brun, Phys. Rev. A **78**, 022324 (2008).
[44] T. Nitsche, S. Barkhofen, R. Kruse, L. Sansoni, M. Štefaňák, A. Gábris, V. Potoček, T. Kiss, I. Jex, and C. Silberhorn, Sci. Adv. **4**, eaar6444 (2018).
[45] A. Romanelli, Phys. Rev. A **76**, 054306 (2007).
[46] B. Skinner, J. Ruhman, and A. Nahum, Phys. Rev. X **9**, 031009 (2019).
[47] M. Montero, Phys. Rev. A **93**, 062316 (2016).
[48] S. Gershgorin, Bull. Acad. Sci. URSS **1931**, 749 (1931).